Electrochemically Treated Film Formation on CoCrMo Alloy for Total Hip Replacement (THR)

BY

SHELLEY KERWELL
B.S., University of Illinois at Chicago, Chicago, 2013

THESIS

Submitted as a partial fulfillment of the requirements
for the degree of Master of Science in Bioengineering
in the Graduate College of the
University of Illinois at Chicago, 2015

Chicago, Illinois

Defense Committee:

Dr. Christos Takoudis, Chair
Dr. Mathew T. Mathew, Orthopedics, Rush University, Advisor
Dr. Kenneth R. Shull, Materials Science and Engineering, Northwestern University
Dr. Markus A. Wimmer, Orthopedics, Rush University

DEDICATION

I would like to dedicate this work and the time invested in the completion of this thesis to my family and friends. My family has encouraged and believed in me during this process. I would also like to dedicate this thesis to the students of the Tribocorrosion Group at Rush University for their mentorship and help, and the facilities provided by Rush University and The Institute of Biomaterials, Tribocorrosion, and Nanomedicine (IBTN) communities.

ACKNOWLEDGMENTS

Primarily, I would like to thank the members of the committee for their invaluable guidance and their educational support in encouraging the thesis process. I would like to thank Dr. Mathew T. Mathew for helping me formulate the project and for his guidance throughout the study. I would like to thank Dr. Kenneth Shull for his valuable discussions and time. I would also like to thank Dr. Christos Takoudis and Dr. Markus Wimmer for their mentorship and insight.

Secondly, I would like to thank David Baer for his help and lessons on electrochemical testing and Rotyslav Kuprienko. I would like to thank Elizabeth Martin from Northwestern University, Evanston, IL for her lessons on the EQCM. I would also like to thank Dr. Yifeng Liao from Northwestern University for conducting Raman spectroscopy on the corrosion samples. I would like to thank Maria F. Alfaro, DDS and Peter Rossman, MS for answering my questions about the tribometer and their help with testing. Thanks to Izabelle Gindri and Dr. Danieli Rodrigues from University of Texas at Dallas, Dallas, TX for performing Atomic Force Microscopy on the corrosion samples. I would like to thank Anirudh Dube and Andrea Bartolini from Ducom Instruments for use of the tribometer and Dr. Takoudis and his NSF-CBET 1067424 Grant for the BioLogic potentiostat and related studies. I would like to thank Dr. Anne George and Amsaveni Ramachandran of The College of Dentistry at UIC for their discussions on protein adhesion and adsorption mechanisms.

Lastly, I would like to thank NSF-FDN 1160951 and The University of Illinois at Chicago, Department of Bioengineering for providing funding and the mentorship provided by the Tribocorrosion Group at Rush University. I would also like to thank The University of Illinois at Chicago and Rush University for providing funding and lab space while conducting experiments.

TABLE OF CONTENTS

TABLE OF CONTENTS (continued)

Chapter Page

LIST OF TABLES

Table Page

LIST OF FIGURES

Figure Page

LIST OF ABBREVIATIONS

Atomic force microscopy	AFM
Bovine calf serum	BCS
Ceramic-on-ceramic	CoC
Cobalt Chromium Molybdenum	CoCrMo
Constant phase element	CPE
Counter electrode	CE
Double layer capacitance (μF)	Cdl
Electrochemical impedance spectroscopy	EIS
Energy dispersive X-ray spectroscopy	EDS
High carbon	HC
Metal-on-metal	MoM
Metal-on-polyethylene	MoP
Open circuit potential (V)	OCP
Polyether ether ketone	PEEK
Potential at Open Circuit	E_{oc}
Potentiostatic	PS
Polarization resistance (ohms•cm^2)	R_p
Reference electrode	RE
Saturated calomel electrode	SCE
Scanning electron microscopy	SEM
Sodium molybdate dihydrate	SMD
Total hip arthroplasty	THA

LIST OF ABBREVIATIONS (continued)

Total hip replacement	THR
Total joint replacement	TJR
Ultra violet Light	UV Light
White light interferometry	WLI
Working electrode	WE
X-ray photoelectron spectroscopy	XPS

SUMMARY

A major concern involving orthopedic implants is their longevity. When implants are placed *in vivo*, the implant and surrounding proteins found within the synovial fluid undergo chemical reactions. These chemical reactions, in part, depend on the implant's bulk and surface material and their reaction to surrounding synovial fluid. In addition, the formation of tribofilm due to tribochemical reactions has been reported. Later, the protective nature of the film was reported against corrosion and wear. However, there are many unknowns in understanding the basic mechanisms of film formation, including its uniformity and homogeneity. Exploring the possibility of forming such tribofilms prior to implantation is a topic of investigation. Therefore, in order to extend implant longevity and prolong implant replacement it is important to investigate the effectiveness of protein concentration on film formation as means to better understand the role of corrosion and wear on orthopedic implants.

The study was conducted in four parts. The purpose of Part 1 of this study is to investigate film formation in a proteinaceous environment through electrochemical treatment and evaluate film effectiveness through electrochemical impedance spectroscopy (EIS). A standard three-electrode corrosion cell was used to conduct the experiments on polished (Ra < 10.0 nm) CoCrMo alloy discs in bovine calf serum (BCS) solution of two different concentrations (0 g/L and 30 g/L protein content) and at four treatment potentials (-0.4 V, +0.6 V, +0.7 V, and +0.8 V). EIS testing (at E_{oc}, potential amplitude: ±10 mV, frequency range: 100 KHz-0.005 Hz) was done before and after the treatment (at potentiostatic conditions) to determine the effects of protein concentration on film formation. The purpose of Part 2, a pilot study, was to determine which formed film in Part 1 had superior tribocorrosion properties using a linearly reciprocating tribometer. A "ball on flat" configuration was used, with a 9.525 mm (3/4 in.) alumina ball for

SUMMARY (continued)

3600 cycles at a frequency of 1 Hz and a weight of 8.4 N. The coefficient of friction during the free potential test was attained during tribocorrosion testing. In Part 3 of the study, sodium molybdate dihydrate (SMD) was added to surrounding electrolyte conditions (30 g/L protein content BCS) to determine the effects of molybdate concentration (8 mM and 32 mM) on the electrochemical behavior of the CoCrMo alloy. In Part 4, a comparison between SMD treatment methods was conducted. Samples were exposed to phosphate buffered saline with 8 mM SMD under UV Light for 24 hrs. and this group was compared to groups that were not UV treated. Electrochemical testing was carried out to determine surface properties.

The results demonstrate an increase in polarization resistance after treatment with increasing protein content. Tribocorrosion results demonstrate film formation lowering the coefficient of friction, while higher SMD concentration increases polarization resistance under UV light. Therefore, the formed electrochemical film may potentially increase the corrosion resistance of THRs in the long term; thus, showing great promise as a pre-surgical treatment that can be applied to implants to increase their longevity *in vivo*.

Keywords: Cobalt-Chromium-Molybdenum, Electrochemical Impedance Spectroscopy, Corrosion, Wear, Protein, Tribocorrosion

I. Introduction

1.1 General Overview of Total Hip Replacement

Total Hip Replacement (THR) procedures have become increasingly performed for the management of hip arthritis among elderly patients and individuals who suffer from degenerative joint disease [1]. In addition to the aging population, there exists a cohort of patients who are younger, active, and have longer life expectancies [2]. Benefits of THR include an increased quality of life among patients, allowing them to continue with improved motility and pain relief. In fact, by the year 2030, the total number of hip replacement procedures performed within the US is projected to increase to 572,000, which is a 174% growth rate compared to the 208,600 number of procedures conducted in 2005 [3].

A typical THR consists of three parts: a femoral component, an acetabular cup, and an articulating interface. Several models of THRs exist; these include THR devices consisting of ceramic, metal, and polymer materials [4]. The general trend towards choosing an appropriate bearing type depends on the lifestyle of the patient [5]. Therefore, for younger patients, the use of ceramic-on-ceramic (CoC) and metal-on-metal (MoM) surfaces are chosen in order to withstand the increased loads on the implant [5]. Specifically, a MoM THR, using the CoCrMo alloy exemplifies traits of biocompatibility, high corrosion resistance, and wear properties, and is therefore used in MoM hip joint devices.

1.2 Total Hip Replacement Material Concerns

Although THR devices do provide a solution to hip arthritis, device concerns still exist. Current issues in hip implants consist of: wear, which is surface and material loss typically occurring due to friction [6] and corrosion, which is the chemical degradation of materials [7]. The synergistic interaction of wear and corrosion processes is termed tribocorrosion [8]. The four major implant wear and tribocorrosion classifications are: CoC bearing wear, polyethylene wear,

taper tribocorrosion, and MoM bearing wear [7]. Polyethylene wear results in polyethylene debris on the submicron scale, causing a histological response in the joint environment [7]. Taper tribocorrosion is the release of metal particles from the taper region of the hip implant [9]. In a review study, MoM bearings exhibited superior implant survivorship compared to CoC or metal-on-polyethylene (MoP) replacements [5]. Additionally, CoC and MoM replacements have demonstrated less wear production and a reduction in the biological response to wear debris [5]. It has also been shown that MoM bearings are able to outlast the 15-year survivorship experienced by MoP bearings [10] and [11].

1.3 Clinical Concerns of Total Hip Replacement

A present challenge in total joint replacement (TJR) is the biological response to material debris [12]. A majority of the debris is resultant of TJR articulating surfaces undergoing *in vivo* corrosion and wear. Through these processes, MoM articulating bearing surfaces are able to release nanometer-sized metal particles [10] and [13].

For patients, complications include hypersensitivity [14], [15], and surface wear, in addition to another clinical concern of osteolysis [5]. The mechanisms and causes of hypersensitivity are still not clearly defined [6]. However, it is understood that hip replacement failure is, in part, resultant of adverse tissue response to wear particles, which causes aseptic loosening of the prosthesis [16]. MoM bearings, comprised of the CoCrMo alloy, have been widely used in total hip replacements, and these too are susceptible to *in vivo* corrosion and wear overtime [10]. Specific concerns of MoM hip replacement include soft tissue inflammation, soft tissue reaction, as well as soft tissue and bone necrosis [7] and [17]. Pseudotumors, or tumor-like masses, are also a reason of concern involving MoM bearing articulation [9], [18], [17], and [19]. CoCrMo particles may even circulate the lymphatic or circulatory systems and end up in regions distant from implant sites [20]. Although after surgery, metal ion levels of cobalt (Co) and

chromium (Cr) are elevated, concerns exist about the potential toxicity and biological impacts on local and systemic migration of these particles [16] and [21].

Campbell et al. conducted a retrieval analysis of total hip arthroplasty (THA) implants. They noted that patients who had MoM bearings in hip implants and demonstrated adverse local tissue reactions (ALTR), resulted in 5 to 40 ppb of cobalt concentration as compared to well-functioning bearings which patients had 2-3 ppb of cobalt concentration [17]. Additionally, it was noted that chromium ion levels were also increased in patients with MoM bearings and ALTR (5-54 ppb), compared to well-functioning THA MoM bearings resulting in 2-3 ppb of chromium concentration [17].

Additionally, Afolaranmi et al., conducted *in vitro* studies in mice using CoCr wear particles of metal implants and found that metal ions may circulate the host system and end up in isolated areas and organs away from the initial implant site [22].

1.4 Tribocorrosion at the Femoral Head and Acetabular Cup Interface

The femoral component of a THA involves a sliding contact with the acetabular component, which results in sliding tribocorrosion [23]. The effects of sliding tribocorrosion are irreversible as the material is lost due to corrosion and wear while in a sliding contact [23]. The CoCrMo alloy has high corrosion resistance partly due to a passive oxide layer (Cr_2O_3) forming on the exposed surfaces. Therefore, the properties of this oxide layer influence the mechanical and chemical interactions at the boundary between the surface of the alloy and the environment [23]. Although this passive layer provides high corrosion resistance to orthopedic metallic biomaterials, it is not able to withstand the effects of sliding tribocorrosion, such as: regional damage, removal of the passive oxide film, and metal particle detachment which causes mechanical wear [23]. Once the surface area re-oxidizes at depassivated regions caused by the movement, metal ions may be released from the surface and a solid oxide may form on the

implant surface [23]. Continual removal of the oxide generates metal particles and ions, leading to biological responses and implant failure [6], [17] and [23].

1.4.1 Tribolayer Findings *in vivo*

It has been recently studied that proteins within the synovial fluid surrounding joint implants can have a profound effect on the corrosion kinetics of MoM implants. However, the interaction between proteins and the implant surface has not been thoroughly investigated [24]. It has been reported that synovial joint proteins, which are largely plasma proteins, may form into layers on implant surfaces, and may help to limit the wear of the implant [25]. These films are termed tribolayers or tribofilms, and were identified on retrieved implants and mechanically tested CoCrMo alloy surfaces using hip simulators [10]. These tribolayers are largely composed of organic carbon, stemming from synovial joint fluid, as well as metal oxides, and salts [10]. It is hypothesized that the tribolayer formation results from mechanical and chemical factors between the upper subsurface and surface of the implant [10]. The components of a tribolayer include the bulk metal surface and the organic material comprising the tribolayer [26].

Wimmer et al., conducted *in vitro* and *in vivo* analyses of tribochemical reactions layers on MoM hip bearings [27]. 80% or more of either the retrieved femoral bearing heads or acetabular cups displayed tribochemical layers [27]. The layers, when present, were predominately located near to the articulating surfaces of the THR bearing [27]. After conducting X-ray photoelectron spectroscopy (XPS) on the tribolayers collected from the retrieved samples, it was shown that tribochemical reaction layers consisted largely of decomposed organic proteins and salts which were deposited onto oxide layers located on the metal surfaces [27]. Other components of the tribolayer may include well-mixed metal and ceramic components [28]. Wimmer et al., concluded that the proteinaceous layer aided in the reduction of surface fatigue since this layer acts like a solid lubricant and is key in keeping low implant wear rates [27].

Specifically, Liao et al., has shown the presence of film formation on retrieved implants consists of a layer that is carbonaceous in its composition [29]. Raman spectroscopy was performed on retrieved hip implants, which identified two peaks that are signature to carbon occurring with Raman shifts at 1383 cm^{-1} and 1580 cm^{-1}. These peaks indicate the presence of graphene, which may help to reduce wear and corrosion at the implant surface by acting as a solid lubricant [29]. However, the mechanisms which enable protein layer formation are still not elucidated [10] and [29]. Wear of the graphitic material may cause a biocompatibility issue if wear leads to the dispersing of graphitic fragments within the pseudo-synovial fluid and present challenges in systemic transport [29].

In 2013, Martin et al. found that carbonaceous films will form on CoCrMo thin films when the alloy is corroded in bovine calf serum via potentiodynamic scans [30]. Mass gain was measured at the alloy surface at potentials near +0.77 V vs. SCE. The films also formed on pure molybdenum thin films during potentiodynamic tests at potentials near +0.06 V vs. SCE, suggesting that molybdenum is necessary to initiate the film formation [30]. X-ray photoelectron spectroscopy (XPS) analysis signified that these films are derived from the serum of proteins because nitrogen was found in the amide or amine states and the nitrogen-carbon ratio was the same as that in serum proteins, including albumin [30]. Although, even with the aid of film initializing components, such as molybdenum, the formed tribolayer layer is not immune to corrosion; and it may breakdown due to chemical interactions, pH changes, fluid composition, wear [29], or other influences.

1.5 Research Questions

The precise mechanism by which these tribolayers form is still under investigation. Research questions that influence the present study include: What are the bonding mechanisms between components of the tribolayer to the metal surface in the presence of proteins? Can

tribolayers be homogeneous, if so, can they be generated *ex vivo* that way? Can these tribolayers be stabilized and generated on a larger scale (i.e. implant surface)?

1.6 Thesis Project

Therefore, in order to address the knowledge gap of hip implant corrosion and tribocorrosion within *in vivo* settings and the influence of tribolayers and additives on implant wear and corrosion, the present study was done in four parts to ensure a well-rounded approach to understand and characterize film formation.

1.6.1 Significance

To understand and better evaluate the limitations on hip implant corrosion, the present study was conducted under four aims. The significance for this work conducted is being able to understand the present limitations of MoM hip implants by investigating the role of film formation during *in vivo* corrosion and tribocorrosion as means to extend implant longevity.

1.6.2 Aims of Thesis Project

The aim of Part 1 is to induce film formation in a proteinaceous environment through electrochemical treatment and then evaluate film effectiveness through electrochemical impedance spectroscopy (EIS). The electrolyte conditions consisted of protein content using bovine calf serum (BCS) under one concentration: 30 g/L protein content. The control electrolyte consisted of a buffer solution of basic solution which had 0 g/L protein content. A custom-built three-electrode electrochemical cell was used to carry out all experiments. Treatment potentials of -0.4 V, +0.6 V, +0.7 V, or +0.8 V were used in addition to the electrolyte condition for each experiment. The treatment step consisted of a 3600 s potentiostatic (PS) test in which the treatment potential was applied. In order to evaluate the surfaces of the alloy before and after the treatment step, EIS tests were conducted. EIS tests were conducted at open circuit both before and after the treatment potential was applied. An equivalent circuit was used to measure the polarization resistance (R_p) and the capacitance of the interaction between the exposed bulk alloy

surface and the surrounding electrolyte. Scanning electron microscopy (SEM), white light interferometry (WLI), atomic force microscopy (AFM), and Raman spectroscopy were performed on the surfaces.

The aim of Part 2, which is a pilot study, was to determine the *in vitro* mechanical properties of the tribolayer under tribocorrosion testing. Tribocorrosion testing was performed on the samples from Part 1 of the study. Part 2 helped to determine which film formation in Part 1 had superior tribocorrosion properties. Tests were done through means of a linear reciprocating tribometer provided by Ducom Instruments. A "ball on flat" configuration with a 9.525 mm (3/8 in.) alumina ball using parameters of 3600 cycles at a frequency of 1 Hz and a normal load of 8.5 N. The evolution of coefficient of friction during the free potential test was attained during the sliding test. The mass loss due to corrosion and wear (K_{wc}) were determined for the samples using WLI.

In Part 3 of the study (similar to Part 1), sodium molybdate dihydrate (SMD) was added to surrounding electrolyte conditions (30 g/L protein content) to determine the effects of molybdate concentration on film formation. Two concentration parameters were chosen of this additive: 8 mM and 32 mM of SMD. These two concentrations signified low and high molybdate concentrations conditions, respectively. The effects of this additive on the electrochemical behavior of CoCrMo alloy were evaluated. An electrochemical corrosion cell was used to carry out the corrosion experiments (the details are comparable to Part 1). EIS (at E_{oc}) was conducted before and after the treatment step, in which the treatment step was done at a constant treatment potential. The treatment potentials used in this part were: -0.4 V, +0.7 V, and +0.8 V. The treatment potential used in Part 1 of +0.6 V was excluded as this treatment potential did not provide a high resistance to corrosion as compared to the other treatment potentials in Part 1.

With this study, an equivalent circuit was used in order to quantify the polarization resistance and the capacitance. SEM and WLI were performed on the samples as well.

The aim of Part 4 was to utilize UV Light as another mean to deposit SMD on film samples. The samples were previously treated using conditions of +0.7 V in 30 g/L protein content under the electrochemical treatment of Part 1. These samples were then soaked for 24 hrs. under UV light with phosphate buffered saline (PBS) with 8 mM SMD. A comparison was made between methods of Part 3 and Part 4 for determining SMD layer deposition. Electrochemical tests were carried out to quantify the polarization resistance and capacitance of the tested conditions.

1.6.3 Hypothesis of Thesis Project

We hypothesize that carbonaceous film formation is influenced by the electrochemical potential and protein content. Therefore, film will form in higher concentrations of protein, promoting a superior resistance to corrosion during *in vivo* conditions. Additionally, higher concentrations of molybdenum ions will help to promote corrosion resistance, as $Mo^{(+6)}$ ions have been shown to initialize film formation on metal surfaces.

2. Electrochemical Behavior of the CoCrMo Alloy: Clinical Relevance (Part 1)

2.1 Introduction

It has been recently studied that proteins within the synovial fluid surrounding joint implants can have a profound effect on the corrosion kinetics of MoM implants. However, the interaction between proteins and the implant surface has not been thoroughly investigated [24]. In some cases, synovial joint proteins, which are largely plasma proteins, are able to form into a layer on the implant surface that helps to limit the wear of the implant [25]. Liao et al., has shown the presence of film formation on retrieved implants consists of a layer that is carbonaceous in its composition. The partially graphitic layer forms a film that helps to reduce wear, corrosion, and friction in addition to helping with the lubrication of articulating surfaces [29]. However, the formed oxide layer is not immune to corrosion; it may breakdown due to chemical attack, pH changes, etc.

In 2013, Martin et al. found that pure thin film molybdenum and the molybdenum found in the thin film CoCrMo alloy while corroding in bovine calf serum using potentiodynamic scans were able to have formation of carbonaceous film [30]. It was seen in this study that at a potential of +0.77 V, a mass gain was seen on CoCrMo thin film surfaces in the presence of 30 g/L BCS [30]. Using XPS, it was shown that the mass gain was derived from serum protein because the nitrogen-carbon ration was the same as that in serum proteins [30].

In 2011, previous work done by our group shows CoCrMo corrosion kinetics are improved in the presence of a specific protein concentration range which results in superior passive film deposition on CoCrMo alloy surfaces [31]. From this previous study, the potentiodynamic curve of the CoCrMo alloy in the tested electrolytes is shown in Figure 2.1. This helped to determine the treatment potentials and the various electrolyte compositions during the electrochemical treatment for the present investigation.

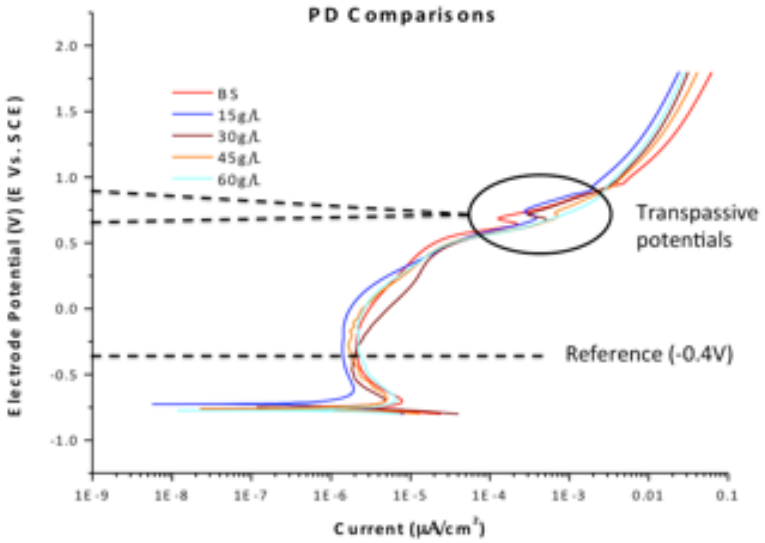

Figure 2.1: Potentiodynamic curve [31]. Indicates transpassive and reference potentials.

Based on the results of Martin, et al., it was hypothesized that potentials within the transpassive regime could induce proteinaceous films on the alloy surface. Therefore, the effect of potential and the protein content on corrosion resistance was tested with electrochemical impedance spectroscopy (EIS). Both before and after the potentiostatic treatment step, EIS was conducted at E_{oc}: During this test, the effectiveness of the film at a normal potential could be evaluated. We hypothesize that carbonaceous film formation is influenced by the electrochemical potential and protein content and effective film will be formed at high concentrations of protein, promoting a superior resistance to corrosion.

In order to extend implant longevity and prolong implant replacement it is important to investigate the effectiveness of protein concentration on film formation as means to better understand the role of corrosion and wear on orthopedic implants.

2.2 Materials and Methods

Sample preparation: 24 high carbon (HC) CoCrMo alloy discs of 12 mm diameter and 3 mm thickness supplied by Alvac Inc., were used in the study. Table I shows the chemical composition of the disc samples. All samples were mechanically polished to a mirror surface finish (Ra < 10.0 nm). Prior to each experiment, the sample was cleaned ultrasonically in 70 % Isopropyl alcohol for 10 minutes and in distilled water for 10 min.

Table I. COMPOSITION OF THE HC COCRMO ALLOY DISCS

Disc Dimensions (mm)		**High Carbon CoCrMo Alloy Chemical Composition (wt.%)**						
Diameter	Thickness	C	Co	Cr	Mo	Si	Mn	Al
12	3	0.034	64.96	27.56	5.70	0.38	0.60	<0.02

Electrochemical treatment: Electrochemical treatment was conducted using a custom-built standard three-electrode electrochemical corrosion cell and a potentiostat (G700, Gamry Inc., Warminister, PA, USA) for the electrochemical treatment. The electrochemical treatment set-up is seen in Figure 2.2. The CoCrMo alloy discs were used as the working electrode (WE) and each disc had 0.38 cm^2 of exposed surface area in the corrosion well. The other two electrodes were a counter electrode made of a graphite rod and a reference electrode, which was a saturated calomel electrode (SCE). A quantity of 10 mL of electrolyte was used for each sample and was warmed to 37 °C. All tests were maintained at the physiological temperature of 37 °C using a water bath during the electrochemical treatment protocol. The composition of the electrolyte is shown in Table II. The experimental design is given in Figure 2.3A of the electrochemical investigation. E_{oc} (free potential) was considered as the EIS potential.

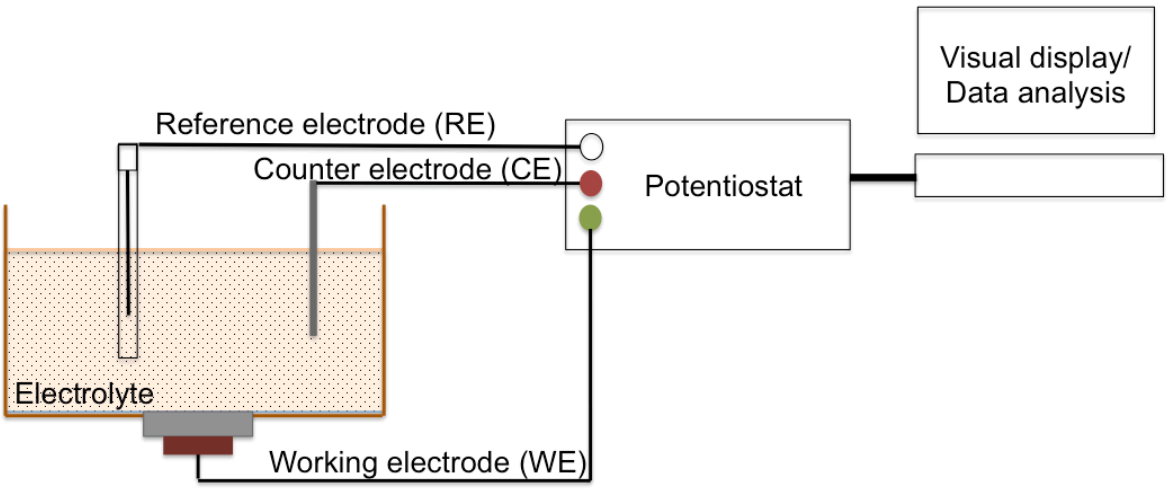

Figure 2.2. Electrochemical corrosion cell. This was used in Part 1 of the study.

Table II. COMPOSITION OF THE ELECTROLYTE

Composition of Bovine Calf Serum (BCS) Electrolyte			
NaCl (g/L)	EDTA (g/L)	Tris (g/L)	Protein (g/L)
9	0.2	27	30

(A)

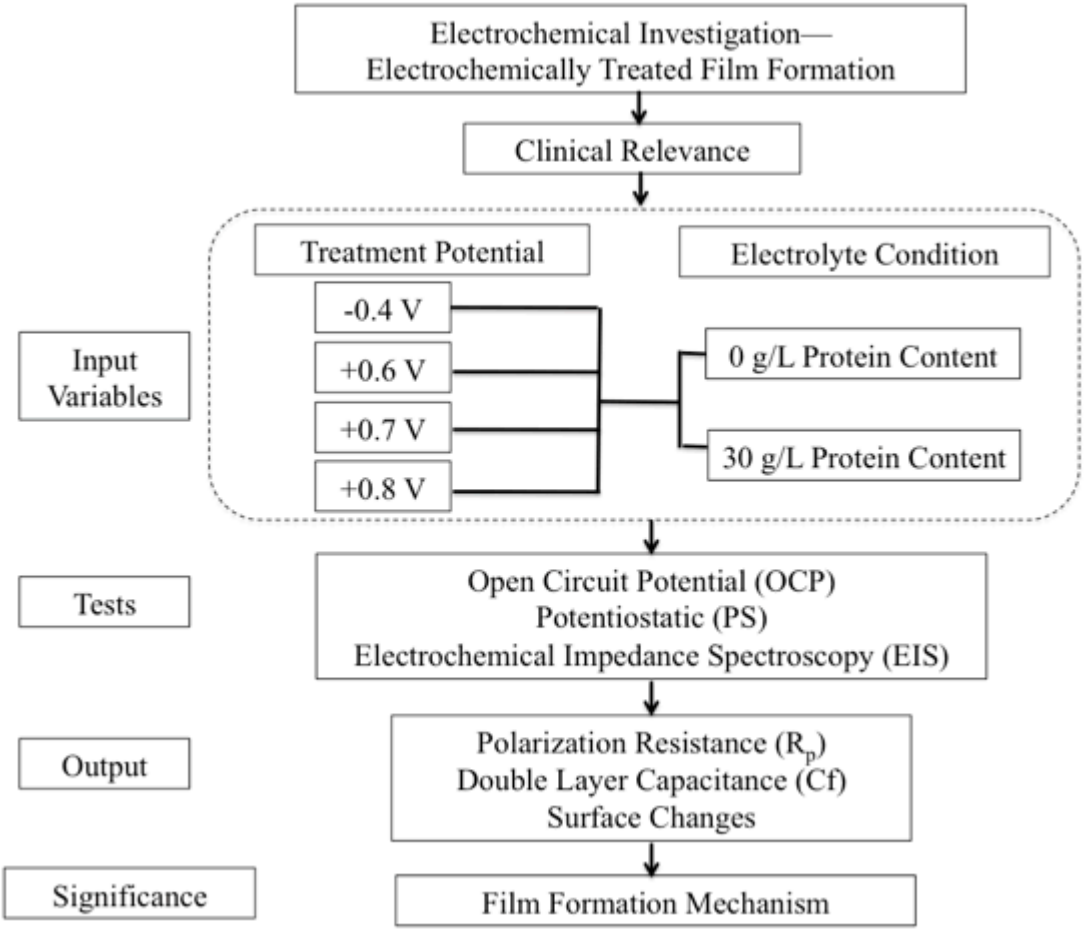

(B)

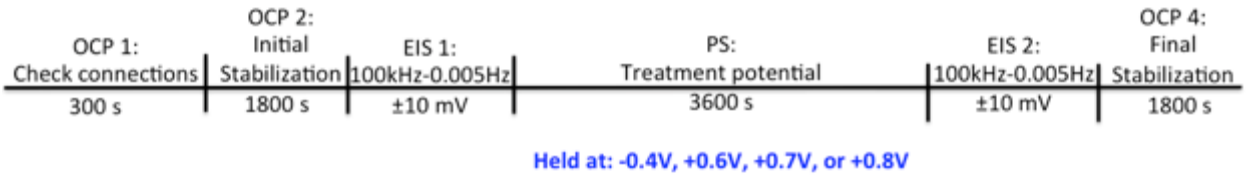

Figure 2.3. Parameters and protocol of Part 1 (A) Schematic of the treatment parameters used in the study, electrolyte condition and treatment potential and (B) Electrochemical treatment protocol for film formation in Part 1.

The first parameter was the treatment potential, which was applied during the treatment step. The values used as potentials were: -0.4 V, +0.6 V, +0.7 V, and +0.8 V. The values of +0.6 V, +0.7 V and +0.8 V were chosen to examine the transpassive regime of the CoCrMo alloy

(Figure 2.1) [31], while the value of -0.4 V was chosen as a control and corresponds to the period of film passivation. The second parameter was the protein concentration in the electrolyte. Protein concentrations of the electrolyte that were used include 0 g/L and 30 g/L protein content of BCS. These values simulate protein concentration during inflammation (30 g/L) [32] and control conditions (0 g/L). For each treatment condition, which is the electrolyte condition and treatment potential, N=3 was conducted.

The entire electrochemical treatment protocol, shown in Figure 2.3B, is as follows: The first test was an open circuit potential (OCP) which assured that the electrochemical cell was set-up correctly based on electrical connections, the second test was a potentiostatic (PS) test done at -0.9 V (cathodic potential), which cleans the surface of the sample from any oxides, which may have formed after the cleaning protocol, the third test was another OCP that allowed the sample to stabilize in the specific conditions of the cell, the fourth test was an electrochemical impedance spectroscopy (EIS), which measured the surface properties of the sample. EIS testing (at treated potential or at E_{oc}, potential amplitude: ±10 mV, frequency range: 100 KHz-0.005 Hz) was done before each treatment step to measure the properties of the material surface and after the application of the treatment step to determine the effects of protein concentration on film formation. The fifth test is another PS, which acts as the treatment step where a specific voltage is applied to the sample (-0.4 V, +0.6 V, +0.7 V, or +0.8 V). The sixth test measures the effect the treatment step on the surface of the material using another EIS (at E_{oc}). The final OCP test measures if there was a change in the open circuit potential based on the electrochemical treatment.

After each experiment the electrolyte was taken out and stored properly, the WE sample was removed and sonicated again using the same cleaning protocol as before the experiment: sonicated for 10 minutes in 70% Isopropyl alcohol and then for 10 minutes using distilled water.

Surface characterization: To determine the surface roughness of each sample, White Light Interferometry (WLI) (Zygo New View 6300, Zygo Corporation, Middlefield, CT, USA) was conducted on three regions of each sample. The surfaces were then imaged using Scanning Electron Microscopy (SEM) (Jeol JSM-6490 LV, Oxford Instruments, Oxford, UK), and Energy dispersive X-ray spectroscopy (EDS) to observe the alloy microstructure and film composition. Atomic force microscopy (AFM) (Bruker Bioscope Catalyst, Billerica, MA, USA) was conducted on the sample to test the generated film's coefficient of friction in dry conditions. Experiments were done with the contact mode technique with a 90° scan angle to the cantilever. The friction amongst the tip and surface was measured as lateral deflections. Images were examined with Bearing Analysis (NanoScope Software) for statistical analysis. Scan areas were 500 nm and a silicon nitride (SCANASYST) probe was used to determine the friction force during the experiments. These probes had a spring constant of k= 0.4 N/m and a frequency of f= 70 kHz. The friction force was calculated by multiplying the resultant lateral deflection voltage signal (subtracting trace from the retrace lateral deflection sensitivity, (S_L)). Raman Spectroscopy (Confocal Raman Spectroscopy, NUANCE, Evanston, IL, USA) was also conducted on the sample surfaces in order to quantify the carbon profile of the generated film for each treatment potential.

2.3 Results

2.3.1 Electrochemical Treatment

The evolution of current during the electrochemical treatment in the potentiostatic test of the treatment protocol is given in Figure 2.4A using 0 g/L protein content and Figure 2.4B using 30 g/L protein content under the four treatment potentials investigated. In Figure 2.4A, it can be seen that the highest to lowest current occur with the following potentials: +0.8 V, +0.6 V, +0.7 V, then -0.4 V, while in Figure 2.4B using the electrolyte of 30 g/L protein content shows the highest to lowest current evolution for the investigated treatment potentials are: +0.8 V, +0.7 V, +0.6 V, then -0.4 V. What is necessary to note is that a current closer to 0 A displays a surface that is more noble, which is shown as +0.7 V in Figure 2.4A and +0.6 V in Figure 2.4B.

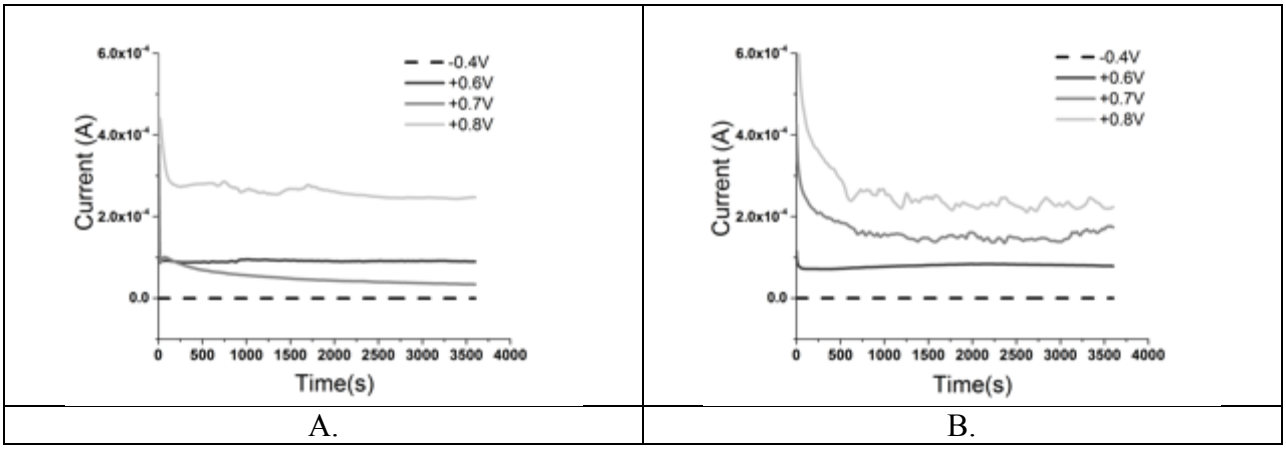

Figure 2.4. Evolution of current (A) The evolution of current as a function of time for each treatment potential in the 0 g/L protein content electrolyte condition and (B) the evolution of current as a function of time for each treatment potential in the 30 g/L protein content electrolyte condition.

2.3.2 Electrochemical Impedance Spectroscopy (EIS) Results

EIS data can be displayed as Bode and Nyquist plots. A Bode plot graphs both the magnitude and phase angle of the total impedance (lZl, (Ohm*cm^2)) versus the frequency (Hz), while a Nyquist plot displays the inverse of the imaginary impedance (-Im(Z), (Ohm*cm^2)

versus the real component of the impedance (Re(Z), (Ohm*cm^2)). Bode and Nyquist plots were graphed for each of the treatment conditions.

Figure 2.5 displays the Bode and the Nyquist plots for the experimental data of Part 1. In Figure 2.5A, the phase angle plot of -0.4 V occurring with 30 g/L protein content indicates superior film formation abilities as compared to 0 g/L protein content. In Figure 2.5B, the Nyquist plot of -0.4 V indicates a larger resistance to corrosion with the 30 g/L protein content electrolyte condition. There are two time constants shown in the +0.6 V Nyquist plot in Figure 2.5C, the first one occurs at lower frequency, while the second one occurs at a mid-range frequency. However, both the electrolyte conditions of +0.6 V appear to overlap throughout the frequency range. Similar to the results of Figure 2.5B, in Figure 2.5D, the 30 g/L protein content electrolyte condition appears to have superior corrosion kinetics compared to the 0 g/L protein content electrolyte condition for the +0.6 V treatment potential. In Figure 2.5E, 30 g/L protein content condition outcomes in superior corrosion kinetics than electrolyte with 0 g/L protein content. In Figure 2.5F, the Nyquist plot of +0.7 V shows that 30 g/L protein content results in superior corrosion kinetics as its plot is steeper than the other electrolyte condition. The Bode plot of +0.8 V, shown in Figure 2.5G, has two time constants. The first is located at the lower frequency and a second, occurs during the mid-range frequency. Both of the electrolyte conditions resulted in separate curves, which only overlap towards higher frequencies. In the Nyquist plot displayed in Figure 2.5H of +0.8 V, shows the 0 g/L protein content electrolyte condition shows superior corrosion kinetics than the electrolyte that has protein. To summarize Figure 2.5, superior corrosion kinetics was demonstrated with +0.7 V than any other anodic potential treatment. The samples treated at +0.7 V demonstrated superior corrosion resistance as compared to the samples treated at all other potentials. It is possible that this occurs because a

proteinaceous film forms under these electrochemical conditions to protect the surface. However the samples treated at +0.7 V without proteins in the electrolyte also demonstrated superior resistance. Therefore, it is likely that an oxide film or other mechanism protects the surface under these conditions.

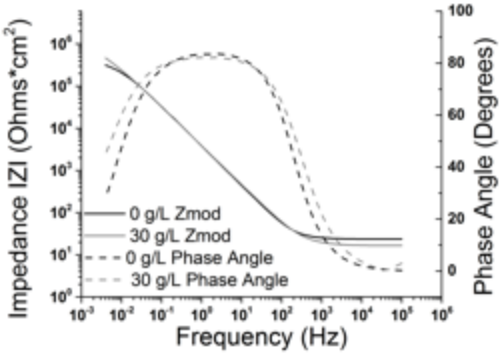

A. -0.4 V Bode Plot

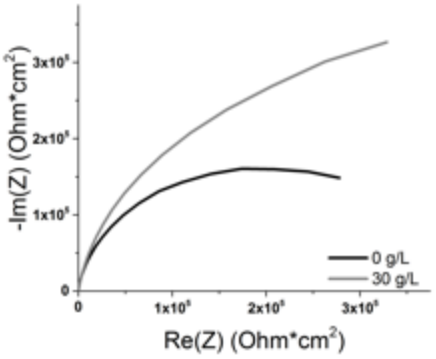

B. -0.4 V Nyquist Plot

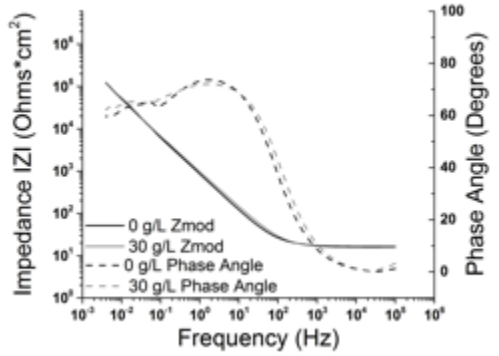

C. +0.6 V Bode Plot

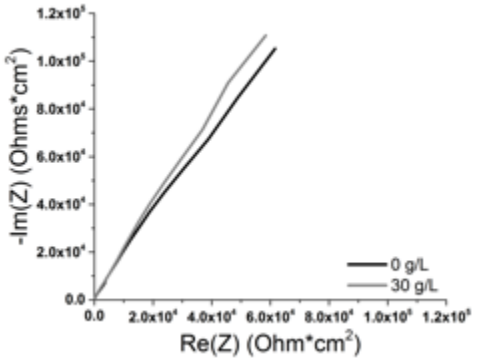

D. +0.6 V Nyquist Plot

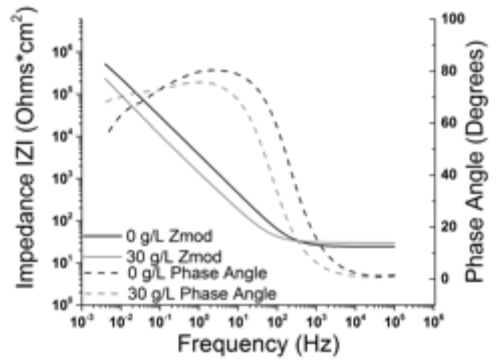

E. +0.7 V Bode Plot

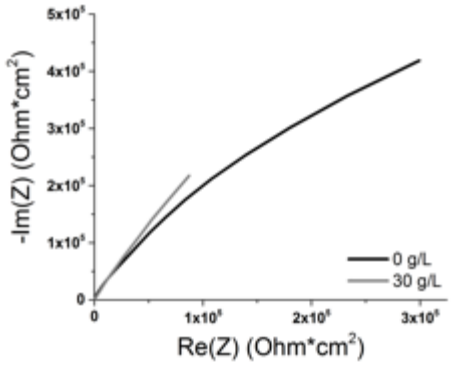

F. +0.7 V Nyquist Plot

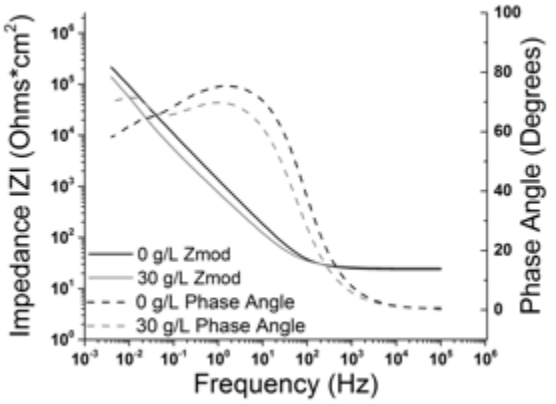

G. +0.8 V Bode Plot

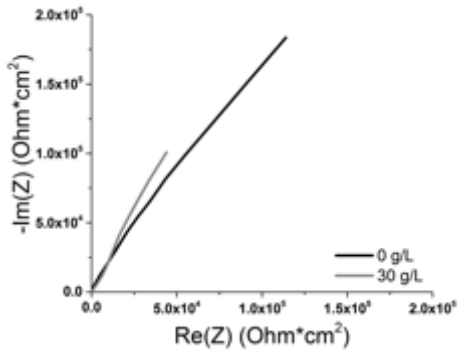

H. +0.8 V Nyquist Plot

Figure 2.5. Bode and Nyquist Plots (A) and (B) Bode and Nyquist plots of -0.4 V, (C) and (D) Bode and Nyquist plots of +0.6 V, (E) and (F) Bode and Nyquist plots of +0.7 V, (G) and (H) Bode and Nyquist plots of +0.8 V.

2.3.2.1 Equivalent Circuit Model

EIS data can be modeled into equivalent circuits to quantify both polarization resistance (R_p) and capacitance. These circuits allow for general trends in electrochemical behavior between the metal and the interactions at the interface of the metal. The Randles Circuit is composed of a resistor in series with a resistor and capacitor in parallel. The first resistor corresponds to the resistance of the electrolyte that the alloy specimen is placed in, while the other two components correspond to the resistance and capacitance of the double layer that forms on top of the metal surface. These values correspond to the bulk metal's resistance to corrosion. The higher the double layer resistance and lower the double layer capacitance outcomes in a metal that is more resistant to corrosion. Since the Randles Circuit is the simplest circuit model, it is not able to explain the complex behavior of the CoCrMo interface in the electrolyte. Therefore, the use of a modified circuit, the Randles Circuit modified with a constant phase element (CPE) was used to substitute the capacitance of the double layer in the original Randles Circuit. The CPE allows for correcting to the ideal capacitance state. Figure 2.6 shows the

equivalent circuit that was used in order to model the experimental data in Part 1. All EIS data in this part were analyzed using the respective equivalent circuit model, as the Chi-squared values were in good agreement with experimental values (≤ 0.002).

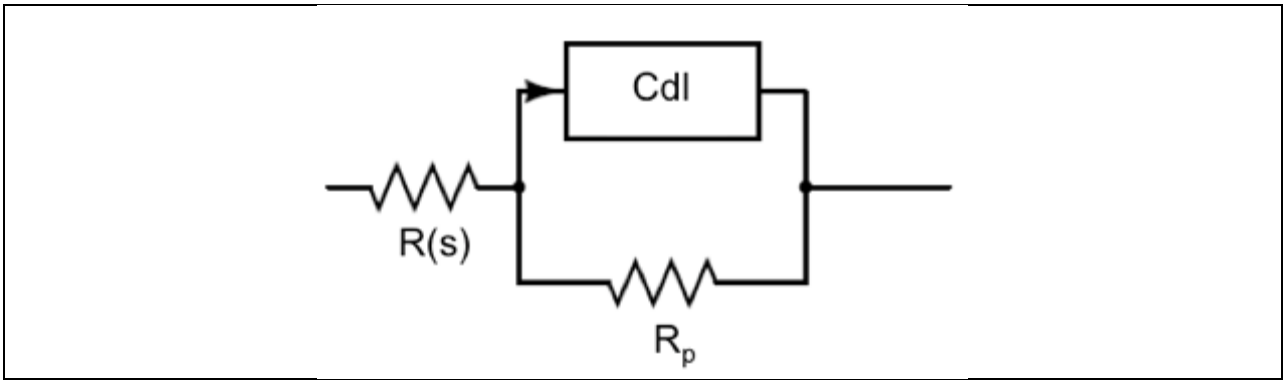

Figure 2.6. Equivalent circuit model. The circuit was the Randles Circuit modified with a constant phase element (CPE).

The evolution of polarization resistance and capacitance are shown respectively in Figure 2.7A and 2.7B using the equivalent circuit in Figure 2.6. In Figure 2.7A, the polarization resistance, R_p, after the treatment step for each potential treatment is shown. As higher resistance is indicative a superior resistance to corrosion, +0.7 V has superior corrosion resistance as compared to other treatment potentials in either 0 g/L protein content or 30 g/L protein content electrolyte conditions. A reason for this is that the potential of +0.7 V occurs in the transpassivation range based on the CoCrMo potentiodynamic curve seen in Figure 2.1 [31].

The opposite is seen in Figure 2.7B, which shows the capacitance after each treatment step at each treatment potential. As a higher value in capacitance corresponds to mitigation in corrosion resistance, +0.6 V and +0.8 V show a higher tendency to undergo corrosion. This may be because these two potentials occur outside of the transpassivation regime in Figure 2.1 [31].

In order to summarize the findings of the resistance and the capacitance of each treatment condition, a ratio of Ra/Rb was taken of resistance after the treatment (Ra) over the resistance before the treatment (Rb). This presented in Figure 2.7C. The ratio of capacitance after treatment (Ca) over capacitance before treatment (Cb), Ca/Cb, is shown in Figure 2.7D. After taking into consideration the ratio of resistance after treatment to resistance before treatment (Ra/Rb) along with the capacitance after treatment to capacitance after treatment (Ca/Cb), the treatment potential that demonstrates superior corrosion kinetics is +0.7 V. This is demonstrated by the larger Ra/Rb ratio in both electrolyte conditions. Although, +0.8 V in 30 g/L protein content displays a Ra/Rb ratio as high as the Ra/Ra of the +0.7 V in 30 g/L protein content treatment condition, the +0.8 V and +0.6 V result in higher Ca/Cb ratios than +0.7 V (Figure 2.7D). This indicates both the aforementioned potentials (+0.6 V and +0.8 V) are outside of the repassivation regime of the alloy.

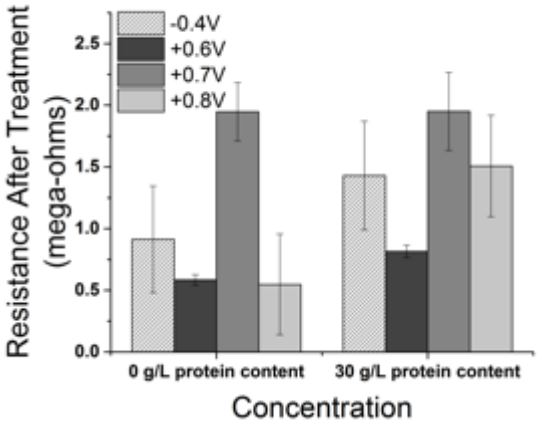

A. Resistance After Treatment in Part 1 using 0 g/L and 30 g/L protein content.

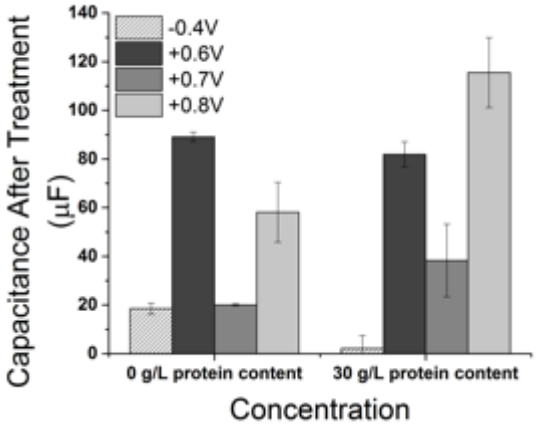

B. Capacitance After Treatment in Part 1 using 0 g/L and 30 g/L protein content.

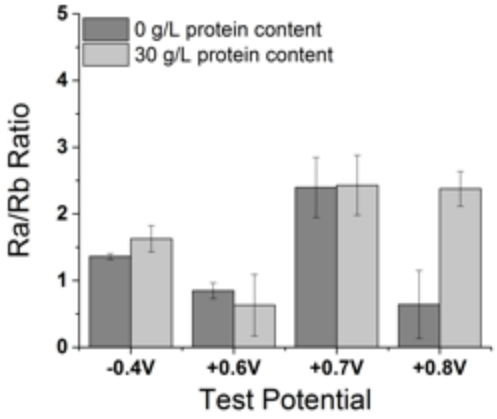

C. Ratio of Resistance After Treatment over Resistance Before Treatment in Part 1.

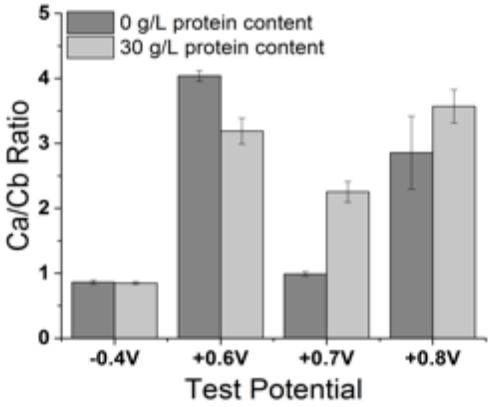

D. Ratio of Capacitance After Treatment over Capacitance Before Treatment in Part 1.

Figure 2.7 Resistance and Capacitance (A) Resistance After Treatment, (B) Capacitance After Treatment, (C) Ratio of Resistance After Treatment over Resistance Before Treatment, (D) Ratio of Capacitance After Treatment over Capacitance Before Treatment.

2.3.3 Surface Characterization Techniques

After the use of equivalent circuit modeling of the data, surface characterization techniques were conducted on the sample surfaces. The primary goal of this characterization was to determine the properties of the surface under four distinctive techniques. Sample surfaces were investigated using WLI, SEM, AFM, and Raman Spectroscopy and their results are found in the following sections.

2.3.3.1 White Light Interferometry

Figure 2.8A-I shows the surface area of each of the samples under their specific treatment potential and electrolyte concentration under WLI. The potential treatment of +0.7 V had the lowest surface roughness was seen with 0 g/L protein content. It is important to note that both electrolyte conditions of +0.8 V outcome in the highest surface roughness, this indicates that there is a significant amount of grain boundary corrosion occurring on the metal surface. Secondly, it is interesting to note that the electrolyte condition of 30 g/L in all the anodic treatment potentials results in a higher surface roughness than the 0 g/L protein content condition for each respective treatment potential. To interpret this finding, it is reasonable to assume that there are more components in 30 g/L protein content than the control electrolyte, which would therefore result in higher surface roughness since the components of the protein might cause uneven film surfaces.

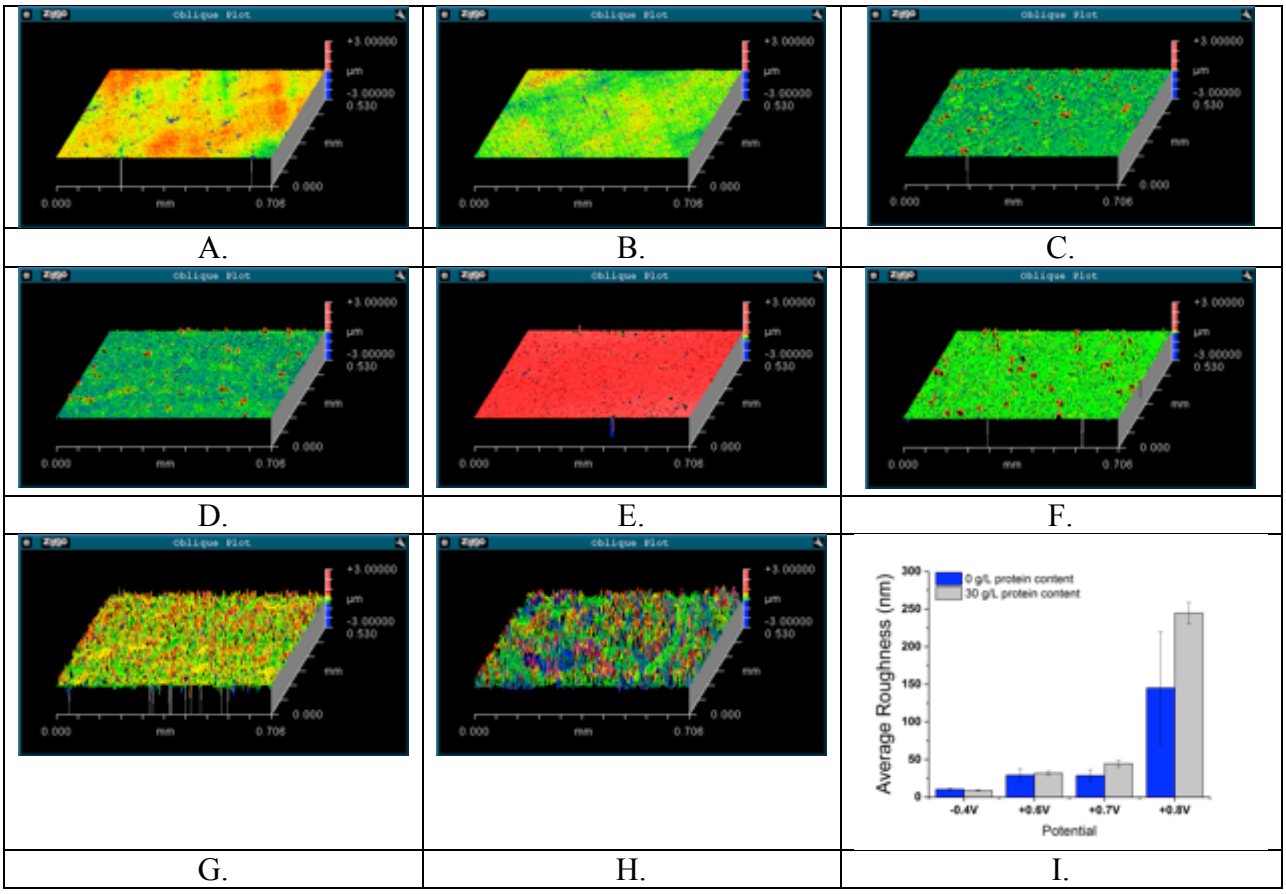

Figure 2.8. White light interferometry (A) -0.4 V in 0 g/L protein content, (B) -0.4 V in 30 g/L protein content, (C) +0.6 V in 0 g/L protein content, (D) +0.6 V in 30 g/L protein content, (E) +0.7 V in 0 g/L protein content, (F) +0.7 V in 30 g/L protein content, (G) +0.8 V in 0 g/L protein content, (H) +0.8 V in 30 g/L protein content, (I) Average Roughness (nm) for each treatment potential and electrolyte condition.

2.3.4 Scanning Electron Microscopy

Scanning electron microscopy (SEM) was conducted on the sample surfaces to evaluate the structure and composition of the surface. SEM results are shown in Figure 2.9A-H for the four treatment potentials in each of the electrolyte conditions, 0 g/L and 30 g/L protein content. Overall, the film and carbonaceous film formation are seen under the SEM images as a darker shade compared to the alloy. Energy dispersive X-ray spectroscopy (EDS) was also conducted on the sample surfaces in order to check the elemental composition of the film in various regions of the surface.

In Figure 2.9A, there is no film formation present, however when this is compared to Figure 2.9B, which shows the same potential in 30 g/L protein content electrolyte condition, there is some carbonaceous film present. It is possible that this film led to the higher Rp value compared to the film shown in Figure 2.9A. Additionally, it is important to note that the treatment potential applied in these two figures, -0.4 V, did not result in significant surface damage of the CoCrMo disc surface since polishing marks are still visible. The SEM images of +0.6 V in 0 g/L and 30 g/L protein content are shown in Figure 2.9C and Figure 2.9D, respectively. There appears to be more homogenous film formation in Figure 2.9D using 30 g/L protein content than 0 g/L protein content as shown in Figure 2.9C. Therefore, it appears that additional protein along with +0.6 V results in a more homogenous surface. In both of these images, there appears to be more grain boundary corrosion than with the treatment potential of -0.4 V. In Figure 2.9E, which is +0.7 V in 0 g/L protein content shows similar results to the condition of +0.6 V in 0 g/L protein content in that these images outcome in uneven film throughout the surface. In Figure 2.9F, which shows +0.7 V in 30 g/L protein content outcomes in extensive carbonaceous film compared to any other treatment. Additionally this potential, in either electrolyte condition, had polishing marks visible similar to the -0.4 V treatment potential, which signifies the subsurface under +0.7 V was not damaged. Lastly, +0.8 V in 0 g/L protein content surface shown in Figure 2.9G resulted in extensive grain boundary corrosion. This indicates the surface was damaged a result of increasing potential. In Figure 2.9H, which shows +0.8 V in 30 g/L protein content shows grain boundary corrosion however it also shows the presence of a carbonaceous layer using EDS. Although this potential outcomes in a proteinaceous layer, grain boundary corrosion and pitting as a result of the increased potential is not a viable potential treatment.

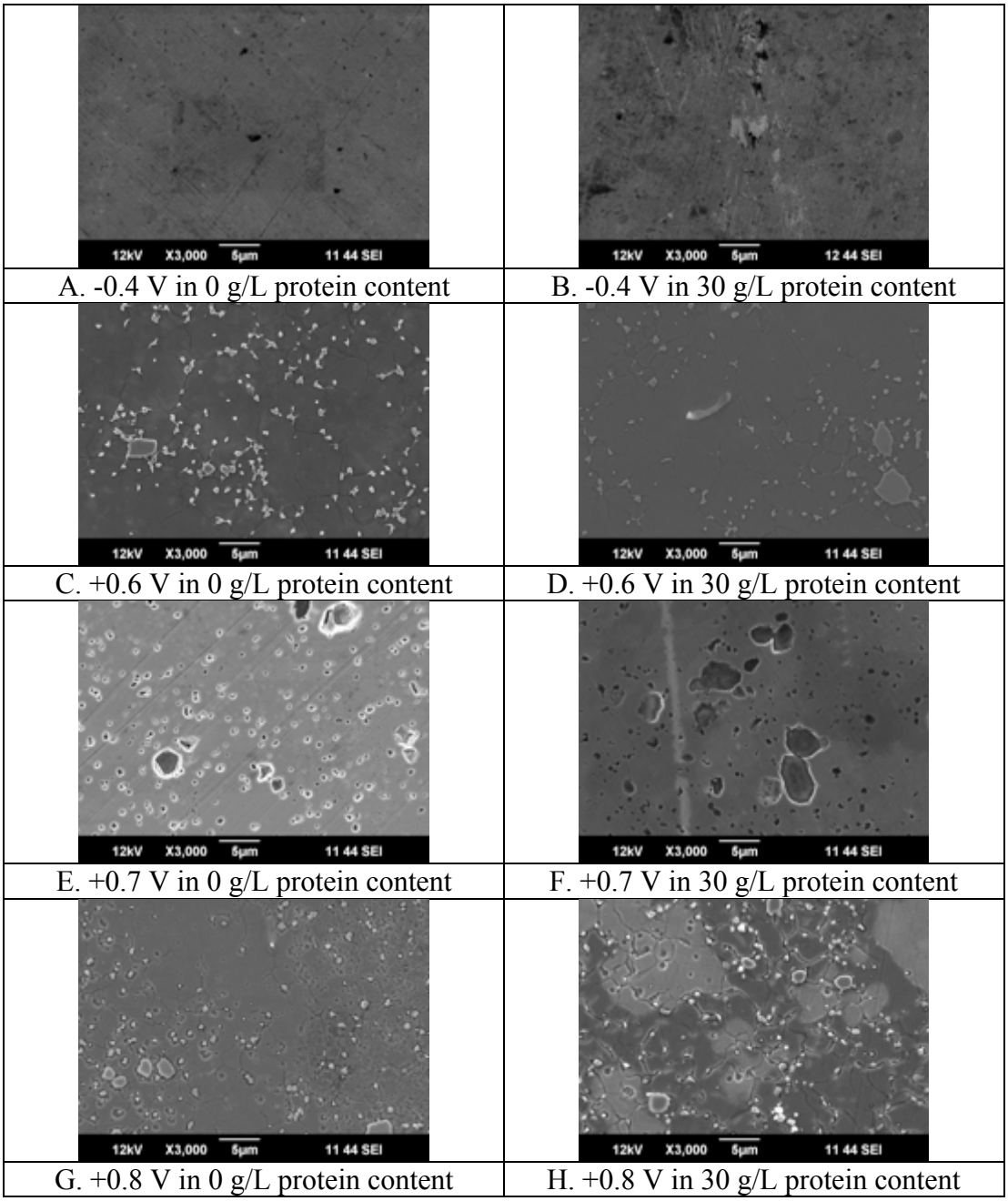

A. -0.4 V in 0 g/L protein content | B. -0.4 V in 30 g/L protein content

C. +0.6 V in 0 g/L protein content | D. +0.6 V in 30 g/L protein content

E. +0.7 V in 0 g/L protein content | F. +0.7 V in 30 g/L protein content

G. +0.8 V in 0 g/L protein content | H. +0.8 V in 30 g/L protein content

Figure 2.9: Scanning electron microscopy (SEM) (A) -0.4 V in 0 g/L protein content, (B) -0.4 V in 30 g/L protein content, (C) +0.6 V in 0 g/L protein content, (D) +0.6 V in 30 g/L protein content, (E) +0.7 V in 0 g/L protein content, (F) +0.7 V in 30 g/L protein content, (G) +0.8 V in 0 g/L protein content, (H) +0.8 V in 30 g/L protein content.

2.3.5 Atomic Force Microscopy

Samples differed in film deposition, which is attributed to the specific electrolyte condition and potential treatment. Therefore, AFM images shown in Figure 2.10A-C help to understand the structure of the film. All samples using 30 g/L protein content as the electrolyte for each potential treatment were investigated. The -0.4 V samples in 30 g/L protein content did not display any grain boundary corrosion on the surface after treatment. Since -0.4 V is the potential corresponding to the passivation of the alloy, this would cause an oxide layer to form instead of a transpassive layer as seen with the positive potential treatments. A larger amount of protein deposition was observed on the +0.7 V in 30 g/L protein content condition compared to other experimental conditions. +0.8 V in 30 g/L protein content displays a relatively homogenous surface. Scanning of the surface for this condition resulted in pits. Overall, pitting features were seen on samples that were treated with positive potential treatments.

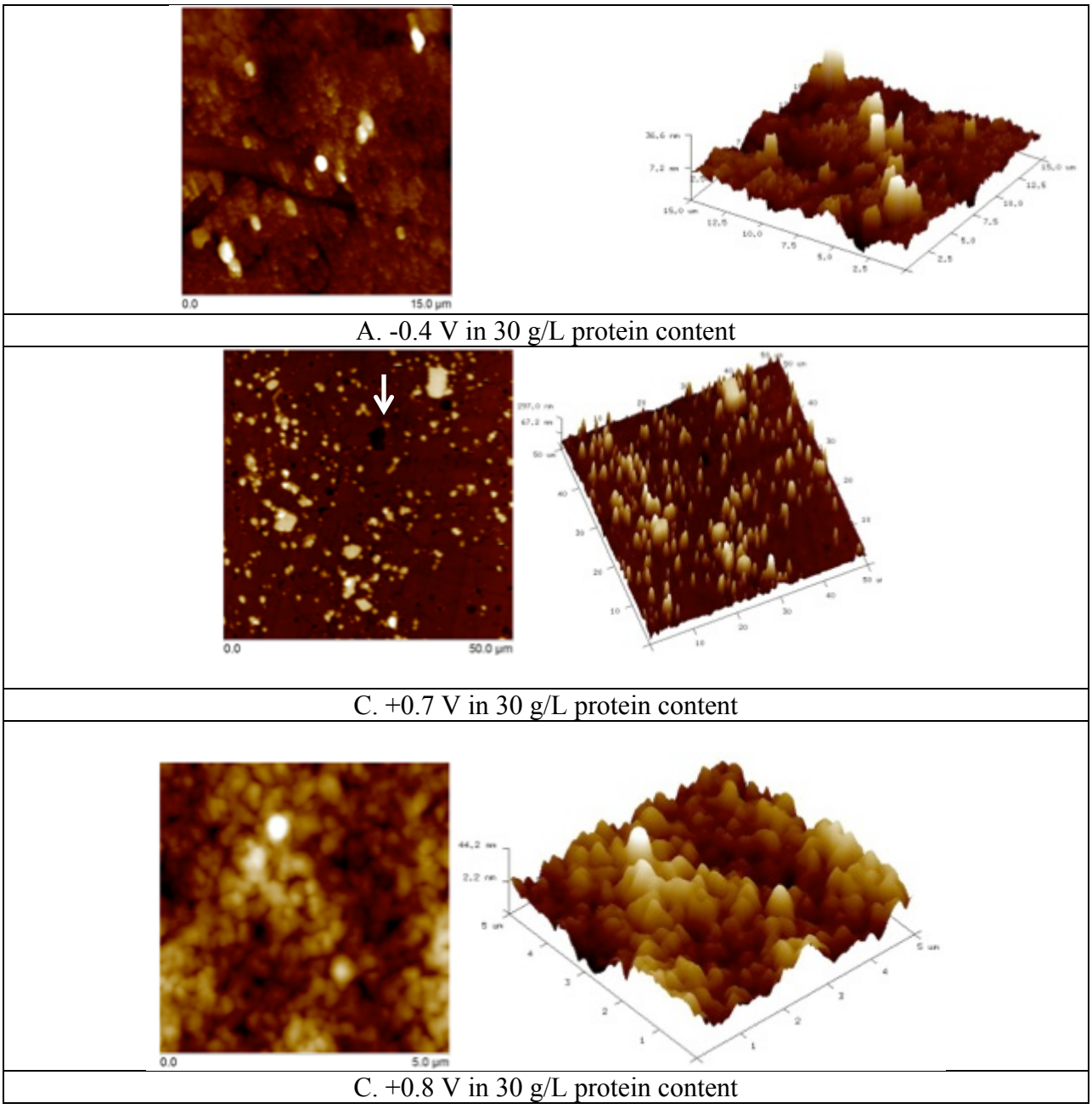

Figure 2.10. Atomic force microscopy (AFM) (A) -0.4 V in 30 g/L protein content, (B) +0.7 V in 30 g/L protein content, (C) +0.8 V in 30 g/L protein content.

The coefficient of friction was also taken at these locations using AFM. The results of this finding are shown in Figure 2.11. All of the samples were taken from the 30 g/L protein content electrolyte condition. The lowest coefficient of friction was demonstrated by the -0.4 V

treatment potential this had a value of 0.109. This may be resultant of the passive oxide film formed on this particular potential treatment. The +0.7 V treatment potential had a coefficient of friction of 0.166, which may be resultant of surface properties. Lastly, potential treatments of +0.6 V and +0.8 V resulted in the highest coefficient of friction using the AFM. It is probable that pitting and metal ion release were able to increase the friction causing a higher coefficient of friction to occur.

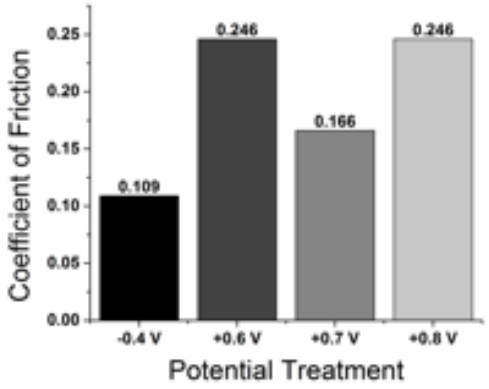

Figure 2.11. Coefficient of friction. This was done using atomic force microscopy.

2.3.6 Raman Spectroscopy

Raman spectroscopy was conducted to understand and quantify the carbon that appears under EDS. This would help to determine which treatment potential outcomes in higher carbon-content film using potential treatments of 30 g/L protein content. Raman spectra were recorded in the range of 1100-1900 cm^{-1}. The typical collection type was 30 s and the results reported were the accumulation of 10-30 measurements. Raman results were obtained using an Action Trivista CRS Confocal Raman system with excitation radiation of an Ar-Kr 514.5 nm gas laser at -10 mW. Raman spectroscopy results are shown in Figure 2.12A-D. The samples that were chosen were of 30 g/L protein content electrolyte condition at each treatment potential. The samples of this electrolyte condition were chosen because it was necessary to determine how

protein would deposit on the alloy surface based on each treatment potential. Previous work has shown the presence of a carbonaceous layer on retrieved articulating surfaces of MoM hip implants occurring at peaks of 1383 cm^{-1} and 1580 cm^{-1} Raman shifts, which comprise the D and G bands, respectively [33]. This carbonaceous layer, or tribofilm, has been suggested to help with limiting friction and protecting implant surfaces under *in vivo* conditions [29]. Figures 2.12C and 2.12D showed clear carbon D and G bands, similar to the graphitic carbon discovered in retrieved MoM hip replacements [29]. The treatments at -0.4 V and +0.6 V did not produce carbonaceous film as their spectroscopy has an absence in the D and G bands. The spectroscopy of -0.4 V and +0.6 V are shown in Figures 2.12A and 2.12B, respectively. Therefore, the potentials investigated in the present study indicate +0.7 V and +0.8 V result in the two peaks that are signature to the presence of the carbonaceous layer. It is interesting to note that +0.7 V in comparison to +0.8 V has a larger intensity of the carbonaceous layer peaks by 100-fold. A higher peak may be indicative of more carbon content found within the film. Therefore, Raman spectroscopy results suggest that the film seen of +0.7 V in 30 g/L protein content shows a high intensity of carbon as compared to the +0.8 V in 30 g/L protein content condition or any other condition investigated.

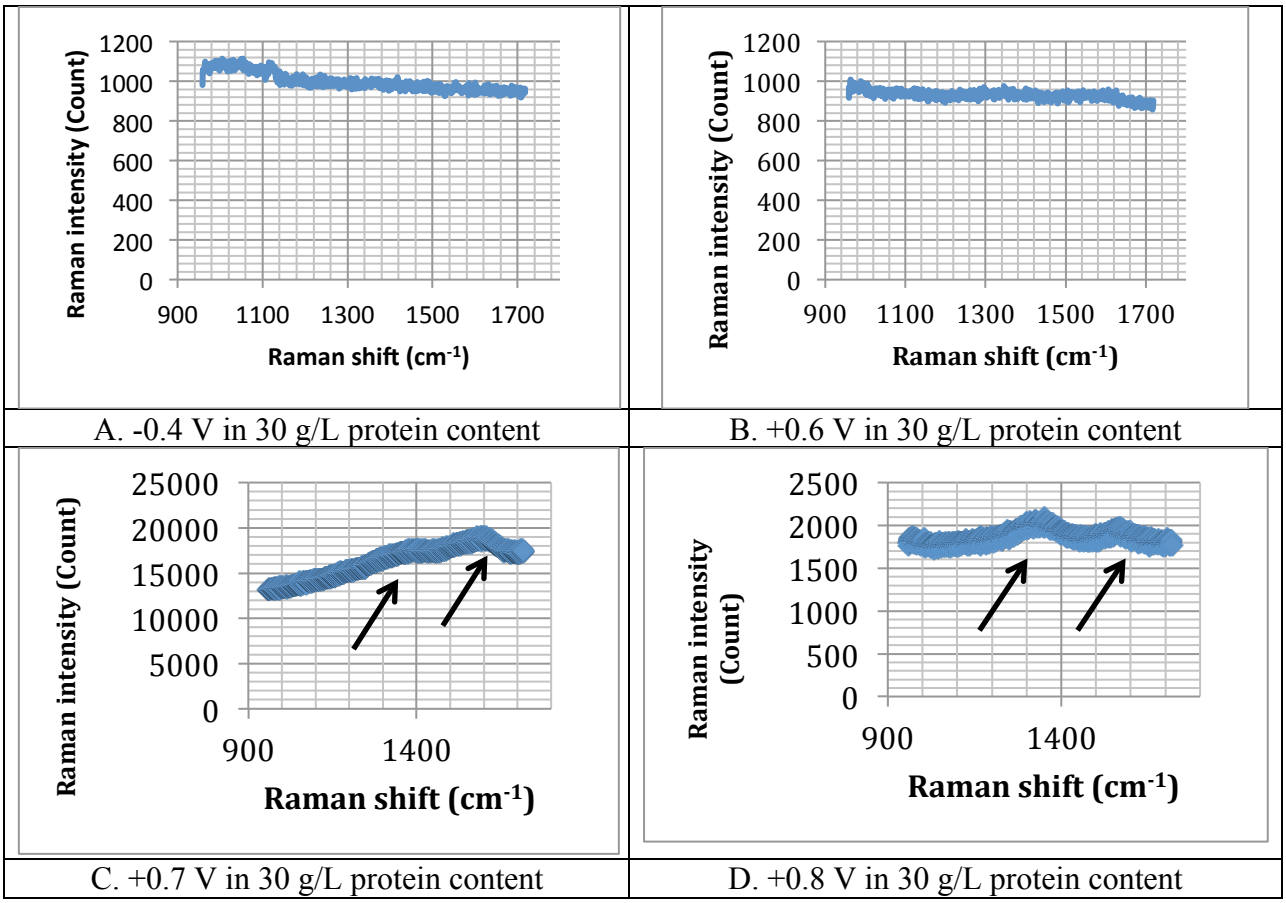

Figure 2.12. Raman spectroscopy (A) -0.4 V in 30 g/L protein content, (B) +0.6 V in 30 g/L protein content, (C) +0.7 V in 30 g/L protein content, and (D) +0.8 V in 30 g/L protein content.

2.4 Discussion

2.4.1 Proposed Film Formation Mechanism

The proposed mechanism of the film formation is shown in Figure 2.13A-D for Part 1. The precise mechanism for *in vivo* loading conditions and kinematics is still not well defined for the generation of a tribolayer [34]. However, based on the parameters of this study, the formation of the film and film characteristics are influenced by, but are not limited to the treatment potential. When corrosion and wear (tribocorrosion) processes occur, the CoCrMo alloy undergoes surface changes. This means that exposed metal ions on the surface of the alloy are able to interact through bonding interactions with the surrounding environment, such as the

synovial fluid because corrosion has caused the surface of the alloy to breakdown resulting in metal ion exposure. The bonding interactions between the exposed metal ions on the surface of the bulk alloy and the surrounding synovial fluid may result in a proteinaceous layer. This may be beneficial for protecting the implant surface from further corrosion processes *in vivo*. However the treatment potential of -0.4 V did not result in any film formation, this can be seen in Figure 2.13A, which has no film present. This potential treatment may produce was able to have an oxide layer which also comprised of metal ions. When comparing the anodic treatment potentials of +0.6 V, +0.7 V, and +0.8 V displayed in Figures 2.13A, B, and C, respectively, show an increase in metal ion release (gray squares). Potentials of +0.6 V and +0.8 V, either resulted in too little or too much metal ion exposure, therefore had less film formation than +0.7 V, as shown with the Raman spectra (Figure 2.12). The potential treatment of +0.6 V did not display peaks of graphitic carbon under Raman spectroscopy, which may indicate that no proteinaceous film formation occurred at this potential. +0.7 V appeared to result in larger carbonaceous film than any other potential, which may be attributed to the amount of metal ions that could bond to components of the protein. After following the treatments at the anodic/transpassive potentials, Raman spectroscopy and SEM with EDS demonstrated film formation using 30 g/L protein content specifically at +0.7 V resulted in a larger amount of carbon and a more homogenous surface compared to other treatment potentials. This phenomenon may have occurred because of an ideal amount of metal ion release since exposing the alloy to potentials of +0.6 V or +0.8 V may have caused too little or too much ion release, not allowing the protein film to form.

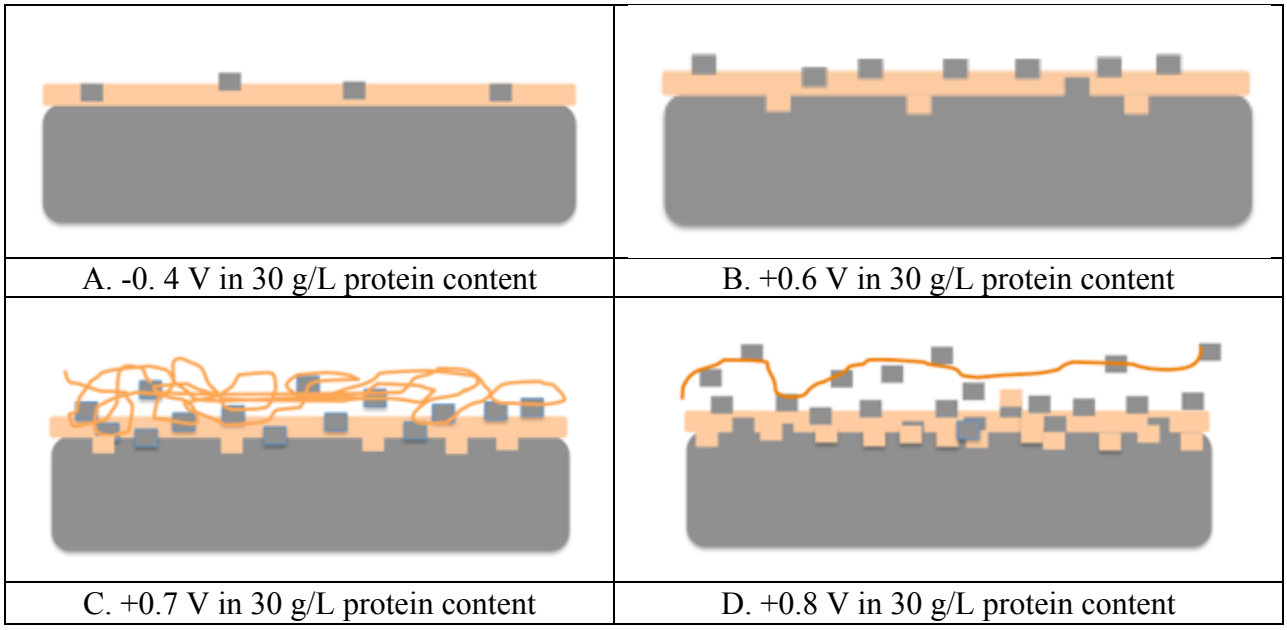

A. -0. 4 V in 30 g/L protein content	B. +0.6 V in 30 g/L protein content
C. +0.7 V in 30 g/L protein content	D. +0.8 V in 30 g/L protein content

Figure 2.13. Proposed mechanism of Part 1 (A) at -0.4 V, (B) at +0.6 V, (C) at +0.7 V, and (D) at +0.8 V.

2.4.2 Clinical Relevance, Limitations, and Future Prospects

Part 1 evaluated electrochemically treated film formation on HC CoCrMo alloy by varying protein concentration and treatment potentials. Orthopedic implant longevity is of concern as *in vivo* corrosion processes may result in metal ion release into the body [26]. The limitations of this study are addressed as follows: there were only two types of protein concentrations used during the experiment: 0 g/L protein content and 30 g/L protein content and only using one type of protein, albumin. Treatment potentials were chosen in whole number increments; therefore, treatments with increments of +0.05 V may be investigated (+0.65 V, +0.75 V, and +0.85 V) for further precision. In addition, the pH of 7.6 was investigated since it is physiologically relevant, however acidic and basic pHs are further parameters to study to simulate pH during inflammation, for example. Conducting XPS on the sample surfaces will help to characterize the adhered film deposition, angles include 90° and 45°. Additionally, it would be of interest to conduct tribocorrosion testing on the samples in order to determine the

integrity of the film formation depending on the treatment potentials and the protein content. The average thickness measurements of the film formation should also be taken into consideration. Further investigations include the utilization of additives in the electrolytic environment that have been linked to induce a tribofilm formation that is resistant to corrosion and determining the film's integrity using tribocorrosion testing techniques.

2.5 Conclusion

The aim of Part 1 was to investigate a treatment condition (treatment potential and electrolyte condition) that will reduce corrosion of implants thus improving their longevity though EIS evaluation and surface characterization techniques. Although the precise mechanism and process for carbonaceous film deposition *in vivo* is still not well understood, this study adds to the general knowledge of how proteins in the synovial fluid affect corrosion kinetics of implants and understanding the role of film formation to provide protection to implant surfaces during *in vivo* conditions. The general conclusions of this study are:

1. +0.7 V as a treatment potential displayed superior corrosion kinetics than +0.6 V or +0.8 V.
2. Increasing protein content using +0.7 V, results in a proteinaceous film that possibly better resists corrosion.
3. Raman spectroscopy analysis displays carbonaceous layer deposition on +0.7 V and +0.8 V in 30 g/L protein content samples, which was absent in -0.4 V and +0.6 V treatment potentials.

3. Tribocorrosion Testing of Film Formation (Part 2)

3.1 Introduction

Tribocorrosion, which is a sub-set of mechanically-assisted corrosion, is an omnipresent concern for load-bearing medical implants [35]. Several factors may influence tribocorrosion of implants, including: contact pressure, lubrication, alloy material, hardness, and material properties [36]. For instance, metallic components of hip joint implants become prone to tribocorrosion as they come in contact with synovial fluid [23] or a corrosive environment [20]. It was reported that after *in vivo* and *in vitro* applications, CoCrMo hip replacements displayed evident corrosion at articulating surfaces and at the taper neck of modular hip replacement devices [37]. Therefore, metal oxides and metal ions are a result of metallic components subject to tribocorrosion [20]. Additionally, after *in vivo* conditions of micro-motion may cease, its effects may continue, causing propagation of corrosion or cracks of the material [35].

In order to limit corrosion *in vivo*, implant devices may be subject to artificial over-passivation, which helps to create a protective oxide layer before implantation [20]. Under sliding conditions, two processes occur: passivation and re-passivation of the oxide layer. The influence of *in vivo* proteins on wear-corrosion interactions was of key investigation since proteins have been shown to affect friction and wear mechanisms of MoM implants [36] and [8]. In fact, over 80% of retrieved hip replacement showed signs of surface tribological film adherence [20]. Yet, it is still unknown how degradation of protein-contained fluid into graphitic carbon under sliding conditions occurs [20]. Therefore, for this study the objective was to determine the tribocorrosion properties of protein film on the surface of CoCrMo alloy discs to simulate hip joint replacements and understand the role of the generated film under tribocorrosion sliding conditions.

3.1.1 Significance

In order to determine how the generated film from Part 1 will withstand *in vivo* conditions, a reciprocating sliding motion was implemented by the tribometer using a loading condition.

3.2 Materials and Methods

Sample preparation: The samples were prepared by using the electrochemical treatment protocol used in Part 1 above. However, prior to each experiment, each sample (already electrochemically treated) was sonicated in 70% Isopropyl alcohol and then in distilled water for 10 min each. The pre-existing samples from Part 1 included treatment potentials of -0.4 V, +0.6 V, +0.7 V, and +0.8 V that were treated in electrolyte conditions using 30 g/L protein content since these would be more physiologically relevant. A new specimen was added to the pre-existing samples, this was a control CoCrMo disc that was polished to ASTM standards with average Ra < 10.0 nm.

Tribocorrosion testing: The samples were subjected to tribocorrosion testing using a tribometer (Advanced Linear Reciprocating Tribometer, Ducom Instruments, Chicago, IL, USA). A custom-built three-electrode polyether ether ketone (PEEK) electrochemical cell was used. The working electrode consisted of the sample with an exposed area of 1.0 cm^2, a SCE was used as the reference electrode, and the counter electrode was a graphite rod. The tribocorrosion testing system is shown in Figure 3.1.

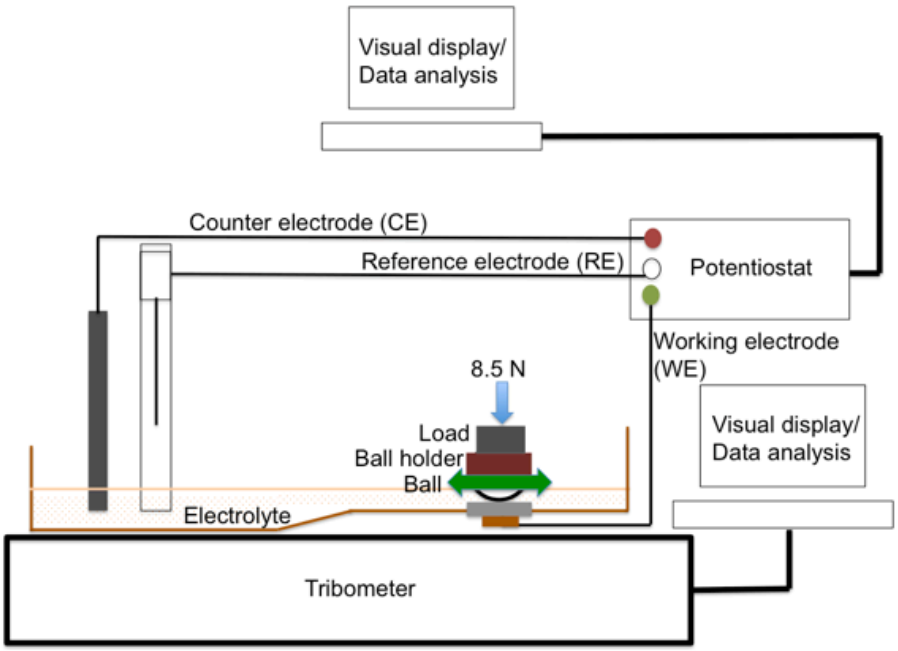

Figure 3.1. Tribocorrosion testing set-up. Testing consisted of an 8.5 N normal load with a sliding distance of 2 mm for 3600 s at 1 Hz.

15 mL of 30 g/L protein content electrolyte was used, with exact preparation and composition as the 30 g/L protein electrolyte from Part 1. EIS was conducted before and after tribocorrosion testing; parameters included a normal load of 8.5 N applied with a "ball-on-flat" configuration. A reciprocating sliding distance of 2 mm at a frequency of 1 Hz for 3600 s was applied using a 9.525 mm diameter alumina ball [Al_2O_3] counter body during the OCP free potential test. The tribocorrosion protocol included an initial OCP (180 s) to test proper connections, a second OCP (1800 s) for initial potential stabilization, an EIS (±10 mV, 100 kHz-0.005 Hz) before sliding, OCP (5000 s, sliding phase), a second EIS (±10 mV, 100 kHz-0.005 Hz) after sliding, and a final OCP (1800 s) for potential stabilization. The experimental protocol is shown in Figure 3.2.

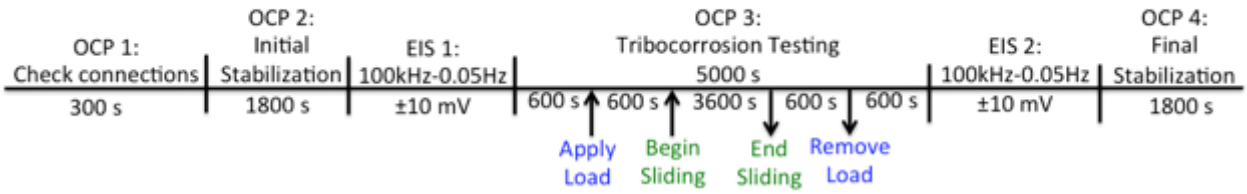

Figure 3.2. Tribocorrosion protocol. This consisted of open circuit potential and electrochemical impedance spectroscopy tests under sliding conditions.

Surface characterization: To determine the loss due to wear, white light interferometry (WLI) (Zygo New View 6300, Zygo Corporation, Middlefield, CT, USA) was utilized for each wear scar. The wear scar was then imaged using scanning electron microscopy (SEM) (Jeol JSM-6490 LV, Oxford Instruments, Oxford, UK), and energy dispersive X-ray spectroscopy (EDS) to observe the microstructure and film composition inside and outside the wear scar.

3.3 Results

The evolution of the coefficient of friction during the tribocorrosion experiment is displayed in Figure 3.3A and the results of the evolution of the potential drop are shown in Figure 3.3B. In Figure 3.3A, the smallest to the largest coefficient of friction is: +0.7 V < +0.6 V < +0.8 V < -0.4 V < Control. A smaller coefficient of friction corresponds to a substance with superior lubricating properties. It is important to note that all previously treated film samples of Part 1 display smaller values of friction coefficients than the Control, which had no film treatment. Therefore, it appears that the previously treated potential treatments provide tribocorrosion superiority over the untreated CoCrMo alloy surfaces. In Figure 3.3B, the average potential during sliding indicates that the +0.7 V potential treatment had the highest (less negative) average potential, while the lowest (more negative) potential average was displayed by the +0.6 V potential treatment. In Figure 3.4A, the potential drop (ΔVd) is shown for each condition when sliding occurred. A larger potential drop signifies a treatment condition that

shows less superiority in tribocorrosion since a higher (more positive) potential corresponds to a more noble material. The largest potential drop was shown in the treatment condition of +0.6 V, while the lowest potential drop was shown with the untreated CoCrMo alloy Control disc. This means that the oxide layer present on the Control condition is able to withstand the primary sliding conditions. However, when looking at the sliding potential (Vs) in Figure 3.4B, it can be seen that the Control and the -0.4 V samples resulted in a very similar average sliding potential. This means that these two conditions have similar behavior under sliding conditions. However, it is important to note the lowest average sliding potential resulted with the +0.7 V treatment potential (which means it is closer to zero, or more noble). The change in recovery potential (ΔVrec), shown in Figure 3.4C, indicates that both the Control and -0.4 V resulted in a potential change that was closer to its starting potential before sliding (see Figure 3.3B). Additionally, from Figure 3.3B, all the conditions either had very similar or lower average potential after sliding. This indicates that after sliding the alloy surface where sliding occurred was not able to recover to the initial potential.

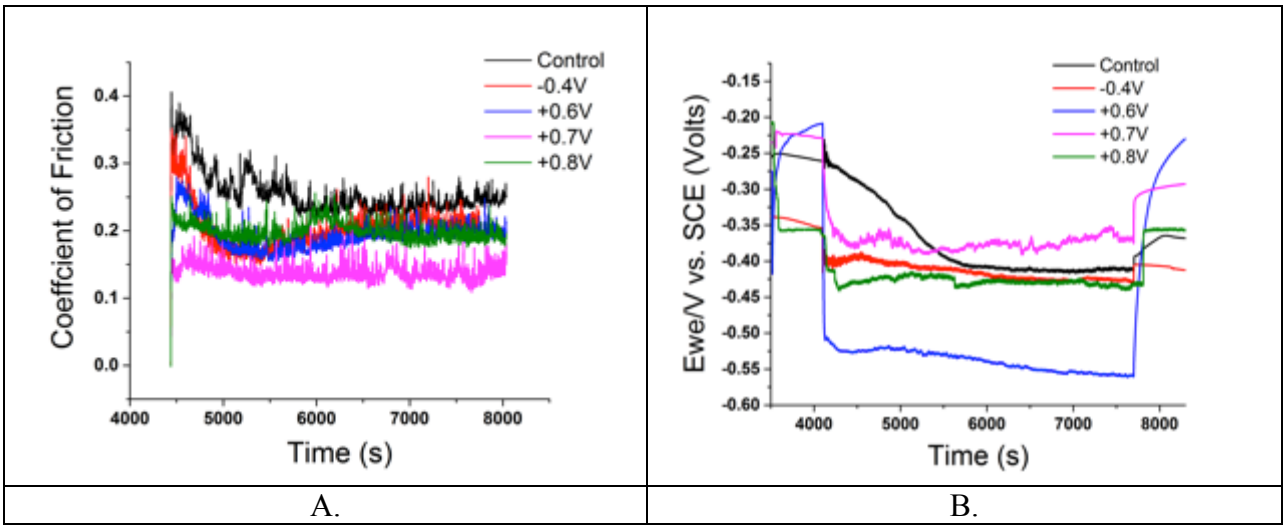

A. B.

Figure 3.3. Tribocorrosion results (A) Evolution of coefficient of friction during the tribocorrosion test and (B) Evolution of potential during the tribocorrosion test.

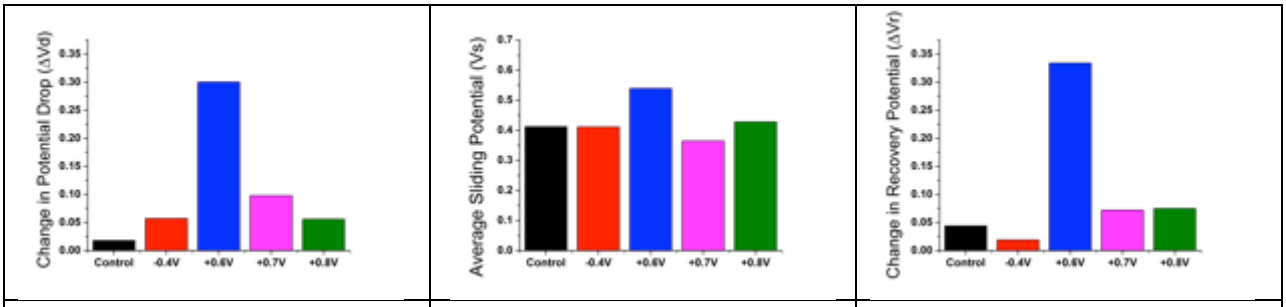

A. B. C.

Figure 3.4. Free potential results (A) The change in potential drop (ΔVd) when the sliding phase begins, (B) the average sliding potential during the sliding phase, and (C) the change in recovery potential (ΔVrec) after the sliding phase ends for all conditions.

From this preliminary data set we can see that the coefficient of friction for the +0.7 V in 30 g/L protein content condition exhibits the smallest coefficient of friction value, in comparison to all other treatment conditions. In order to measure the volume of the wear loss due to tribocorrosion testing, WLI was conducted on each wear scar in the Control and the +0.7 V in 30 g/L protein content condition. The plots of the wear scar for the two conditions shown in Figure 3.5A-B. The total volume loss (μm^3) for each condition is 2.07×10^{-7} μm^3 and 1.98×10^{-7} μm^3 for the Control and +0.7 V in 30 g/L protein content conditions, respectively. The SEM images post-sliding of inside and outside the wear scar for each condition are shown in Figure 3.6A-J. Wear scar images, shown in Figures 3.6A, 3.6C, 3.6E, 3.6G, and 3.6I, indicate that there is no film formation post-sliding. This was verified by energy dispersive X-ray spectroscopy (EDS), which measured less carbon and molybdenum occurrence in these regions. Additionally, when comparing the wear scar images to their respective images outside of the wear scar for each condition show that film formation remained from Part 1 (Figures 3.6B, 3.6D, 3.6F, 3.6H, and 3.6J). However, in Figures 3.6F, 3.6H, and 3.6J, grain boundary corrosion did occur in the

anodic potential treatments. It was also observed that increasing the anodic potential appeared to increase the grain boundary corrosion.

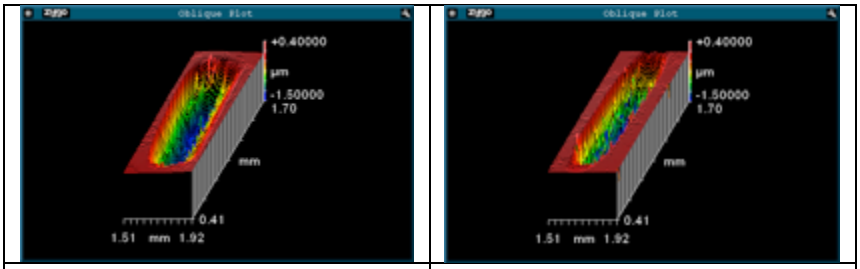

A. B.

Figure 3.5. Wear scar plots (A) Control and (B) +0.7 V in 30 g/L protein content.

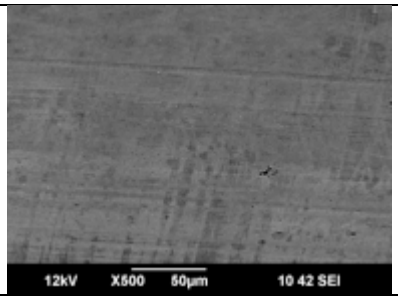

A. CoCrMo Control (inside the wear scar).

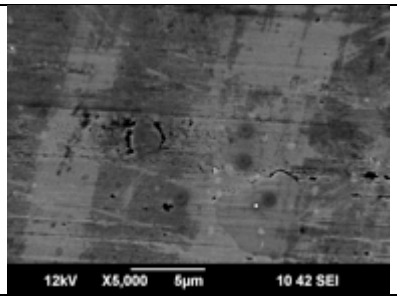

B. CoCrMo Control (outside the wear scar).

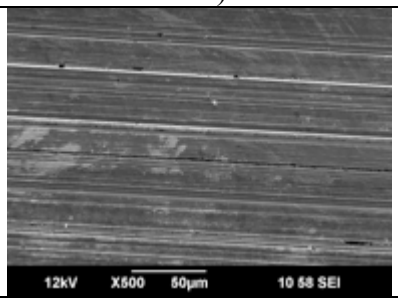

C. -0.4 V (inside the wear scar).

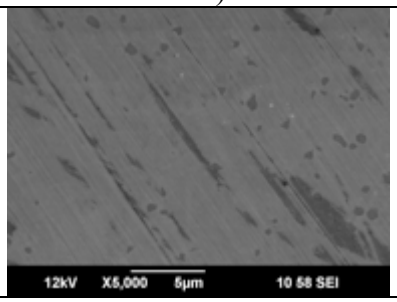

D. -0.4 V (outside the wear scar).

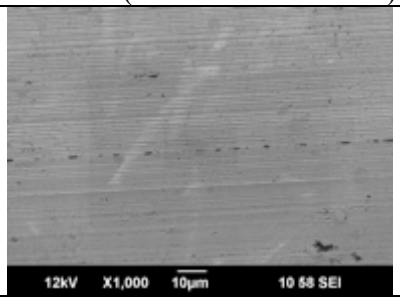

E. +0.6 V (inside the wear scar).

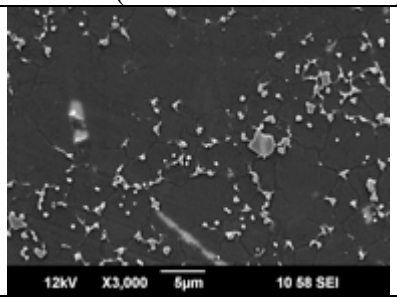

F. +0.6 V (outside the wear scar).

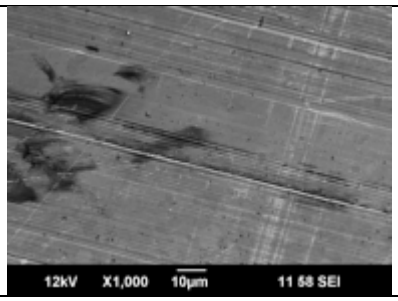

G. +0.7 V (inside the wear scar).

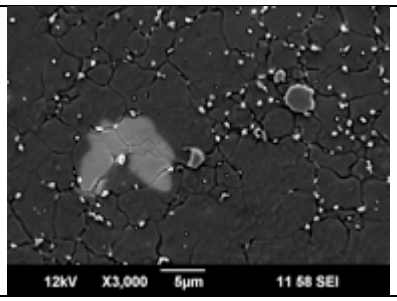

H. +0.7 V (outside the wear scar).

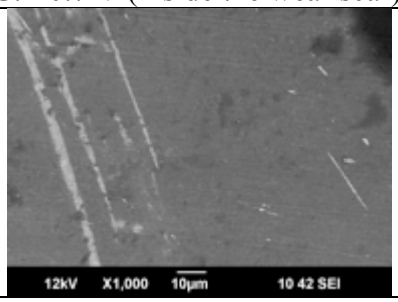

I. +0.8 V (inside the wear scar).

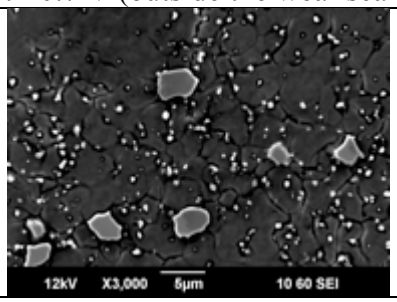

J. +0.8 V (outside the wear scar).

Figure 3.6. Scanning electron microscopy (SEM) (A) Control, inside the wear scar, (B) Control, outside the wear scar, (C) -0.4 V in 30 g/L protein content, inside the wear scar, (D) -0.4 V in 30 g/L protein content, outside the wear scar, (E) +0.6 V in 30 g/L protein content, inside the wear scar, (F) +0.6 V in 30 g/L protein content, outside the wear scar, (G) +0.7 V in 30 g/L protein content, inside the wear scar, (H) +0.7 V in 30 g/L protein content, outside the wear scar, (I) +0.8 V in 30 g/L protein content, inside the wear scar, and (J) +0.8 V in 30 g/L protein content, outside the wear scar.

3.4 Discussion

Based on the preliminary tribocorrosion results displayed in Figure 3.3A, the sample of +0.7 V in 30 g/L protein content exhibits the lowest coefficient of friction during the sliding with an average of 0.138. This infers the electrochemical treatment at +0.7 V during Part 1 has superior lubricating properties than the Control in addition to the other treatment potentials used in Part 1. This comparison shows that a proteinaceous layer may be advantageous for providing a lower coefficient of friction, thus improving lubricating phenomena. Not only was there a smaller value in the coefficient of friction for the +0.7 V in 30 g/L protein content condition, a lower potential drop was additionally seen in Figure 3.3B. The +0.6 V in 30 g/L protein content

exhibits the lowest potential drop during the tribocorrosion testing, indicating the electrochemical treatment from Part 1 may have no advantage over protecting the surface of the bulk alloy from wear. The samples of -0.4 V and +0.8 V appear to have superior tribocorrosion properties than +0.6 V.

This suggests the electrochemical treatment of Part 1 using the parameters of +0.7 V in 30 g/L protein content appears to have a benefit of lowering the coefficient of friction. However, collectively, all the samples that were previously treated displayed coefficient of friction values lower than that of the Control sample, which had no film deposition. This shows the presence of protein adsorption helps to reduce the coefficient of friction during the tribocorrosion testing. Based on the evolution of potential during tribocorrosion testing for each of the treatment potentials (Figure 3.3B), the lowest potential drop was seen with the +0.7 V potential, which further signifies the film formed during Study 1 appears to provide superior corrosion resistance. The largest potential drop that was seen was with the +0.6 V treatment condition, which is expected, as this is the pitting potential of the alloy.

In Figure 3.4B, it can also be verified that the +0.6 V treatment condition had the lowest (more negative) potential during sliding, indicating that this treated film was not able to withstand the mechanical sliding conditions occurring. However, while the sliding occurred, the +0.7 V treated film resulted in an average sliding potential closest to zero, indicating its more noble properties. The other treated film to display a lower change in potential drop was the +0.8 V treated film (Figure 3.4A).

The WLI images of the wear scar are shown in Figure 3.5A-B for the Control and +0.7 V treatment potential. The Control sample resulted in 2.07×10^{-7} μm^3 of volume loss, while the +0.7 V in 30 g/L protein content shows a volume loss of 1.98×10^{-7} μm^3. Since the volume of wear

shown in the Control tends to be greater than the treated sample, the film formation on this treated sample appears to help with minimizing the wear loss during tribocorrosion testing. Wear loss measurements confirm coefficient of friction and free potential results during tribocorrosion testing correspond to film formation providing the treated surface (+0.7 V) with protection from the tribocorrosion testing parameters in Part 2.

Figure 3.6A-J shows the SEM images inside and outside the wear scar after sliding for each condition. A key aspect of Figures 3.6C, 3.6E, 3.6G, and 3.6I show that the film formation was not able to regenerate during tribocorrosion sliding conditions since SEM images show an absence of film inside the wear scar compared to the respective images of each treatment outside of the wear scar. Figures 3.6F, 3.6H, and 3.6J show the surfaces outside the wear scar for treatments of +0.6 V, +0.7 V, and +0.8 V, respectively. From these figures it appears that increasing the treatment potential from -0.4 V (Figure 3.6D), then from positive anodic potentials of: +0.6 V, +0.7 V, and +0.8 V, result in higher amounts of grain boundaries and carbides. This may explain the mechanism of film formation during Part 1 of the study, in that a higher release of metal ions may cause less film formation to occur.

3.5 Conclusion

The next step includes conducting more trials to further provide results based on the preliminary experiments of Part 2. In addition, conducting experiments in 0 g/L protein content as the electrolyte in Part 2 to determine the effects of protein condition on film formation tribocorrosion properties in contrast to no protein conditions. From this study, the following conclusions are:

1. The treatment potential of +0.7 V displays the lowest average sliding potential (Vs) and the lowest coefficient of friction.

2. Treated film at +0.7 V helped to decrease the wear loss compared to the Control sample.

3. All of the previously treated samples (-0.4 V, +0.6 V, +0.7 V, and +0.8 V) did not result in film re-formation after sliding (verified by SEM images), therefore increasing the sliding time may result in film formation under sliding conditions as 3600 s may not have been enough time for the film to re-form.

4. Electrochemical Behavior of CoCrMo Alloy Under Various Sodium Molybdate Dihydrate (SMD) Concentrations (Part 3)

4.1 Introduction

In 2013, Martin et al. found that pure molybdenum thin film and CoCrMo thin when corroded via potentiodynamic scans were able to form carbonaceous film in the presence of a proteinaceous electrolyte [30]. It was seen in this study that at a potential of +0.77 V, a mass gain was seen on the surfaces on the CoCrMo thin film [30]. Using XPS, it was shown that the N-C ratio was that of serum protein, albumin [30]. Therefore, in Part 3, sodium molybdate dihydrate (SMD) was added into the electrolyte condition of 30 g/L protein content to determine the effects of the molybdate ion on the alloy corrosion properties, as molybdenum may be important for film initialization. Specifically, the concentration of 8 mM SMD and 32 mM SMD were added to the 30 g/L protein content electrolyte. 8 mM SMD was chosen based on an initial estimate of the molybdate concentration at the time of the first protein deposition during corrosion of a pure Mo thin film [30].

4.2 Materials and Methods

Sample preparation: 24 HC CoCrMo alloy discs of 12 mm diameter and 3 mm thickness supplied by Alvac Inc., were used in this part of the study. Like the samples of Part 1, all samples of Part 3 were mechanically polished to a mirror surface finish (Ra < 10.0 nm). Prior to each experiment, the sample was cleaned ultrasonically in 70% Isopropyl alcohol for 10 minutes and then in distilled water for 10 min. Electrolyte composition consisted of 30 g/L protein content of BCS. The additive used was white crystals of sodium molybdate dihydrate (SMD, $Na_2MoO_4 \bullet H_2O$) (Sodium molybdate dihydrate - ACS reagent, ≥99%, 331058 Sigma-Aldrich Co. LLC, Saint Louis, MO, USA). Concentrations of SMD included 8 mM or 32 mM, which were dissolved in 30 g/L protein content solution.

Electrochemical treatment: Electrochemical treatment was conducted using a standard three-electrode corrosion cell (Figure 2.2). The CoCrMo alloy discs were used as the working electrodes (WE) and each disc had 0.38 cm^2 of exposed surface area in the corrosion well. The other two electrodes were a graphite rod counter electrode and a SCE reference electrode. A quantity of 10 mL of electrolyte was used for each sample and was warmed to 37 °C. All tests were maintained at the physiological temperature of 37 °C using a water bath during the electrochemical treatment. Treatment potentials were -0.4 V, +0.7 V, and +0.8 V. The potential of +0.6 V was not chosen since the results of Part 1 of this treatment potential did not indicate any the presence of carbonaceous film under Raman spectroscopy. The second parameter was the protein concentration in the electrolyte surrounding the electrodes. The electrolyte composition included 30 g/L protein content of BCS. Since the aim of Part 3 was to determine the effects of SMD on mechanisms of film formation, the electrolyte conditions included either 8 mM or 32 mM of SMD to represent conditions of elevated molybdenum concentration. For each electrolyte condition and treatment potential N=3 was conducted.

The entire electrochemical treatment protocol is comparable to Part 1 of this study, shown in Figure 4.1. However, just to reiterate: the first test was an open circuit potential (OCP) which assured that the electrochemical cell was set-up correctly based on electrical connections, the second test was a potentiostatic (PS) test done at -0.9 V (cathodic potential), which cleans the surface of the sample from any oxides, which may have formed after cleaning, the third test was another OCP that allowed the sample to stabilize in the specific conditions of the cell, the fourth test was an EIS test, which measured the surface properties of the sample. EIS testing (at E_{oc}, potential amplitude: ±10 mV, frequency range: 100 KHz-0.005 Hz) was done before each treatment step to measure the properties of the material surface and after the application of the

treatment to determine the effects of protein concentration on film formation. The fifth test is another PS, which acts as the treatment step where a specific voltage is applied to the sample (-0.4 V, +0.7 V, or +0.8 V). The sixth test measures the effect the treatment step on the surface of the material using another EIS (at E_{oc}). The final OCP test measures if there was a change in the potential based on the electrochemical treatment.

After each experiment the electrolyte was taken out and stored properly, the WE sample was removed and sonicated again using the same cleaning protocol as before the experiment: sonicated for 10 min in 70% Isopropyl alcohol and then for 10 min using distilled water.

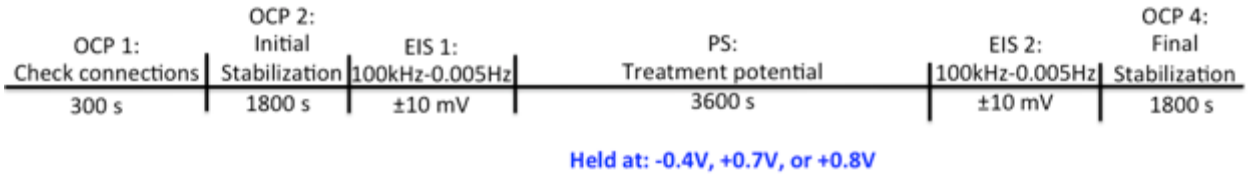

Figure 4.1. Electrochemical treatment protocol. This consisted of using treatment potentials of -0.4 V, +0.7 V and +0.8 V in either 8 mM or 32 mM of sodium molybdate dihydrate.

Surface characterization: To determine the average surface roughness (Ra) of the induced film formation, White Light Interferometry (WLI) (Zygo New View 6300, Zygo Corporation, Middlefield, CT, USA) was utilized in three spots for each sample. The surfaces were then imaged using Scanning Electron Microscopy (SEM) (Jeol JSM-6490 LV, Oxford Instruments, Oxford, UK), and Energy dispersive X-ray spectroscopy (EDS) to observe the alloy microstructure and film composition.

4.3 Results

The results of EIS after the treatment are given in Figure 4.2A-D, for the two concentrations of SMD in each of the three treatment potentials. In Figure 4.2A, the Bode plot using 8 mM for each treatment potential is shown. It indicates that the both the positive treatment potentials outcome in two time constants, the first located at a lower frequency and the second, at the mid-range frequency. The Nyquist plot in Figure 4.3B for the same treatment conditions demonstrate superior corrosion kinetics using +0.7 V as the treatment potential in comparison to -0.4 V or +0.8 V. The Bode plot using 32 mM SMD for the treatment potentials is given in Figure 4.2C. It also shows two time constants for +0.7 V and +0.8 V treatment potentials located at low and mid-range frequencies. While the -0.4 V Bode plot has only one time constant in the mid-range frequency. Similar to the Bode plot of 8 mM SMD, the Nyquist plot of 32 mM SMD, displayed in Figure 4.2D indicates the +0.7 V treatment potential results in superior corrosion kinetics than the other treatment potentials.

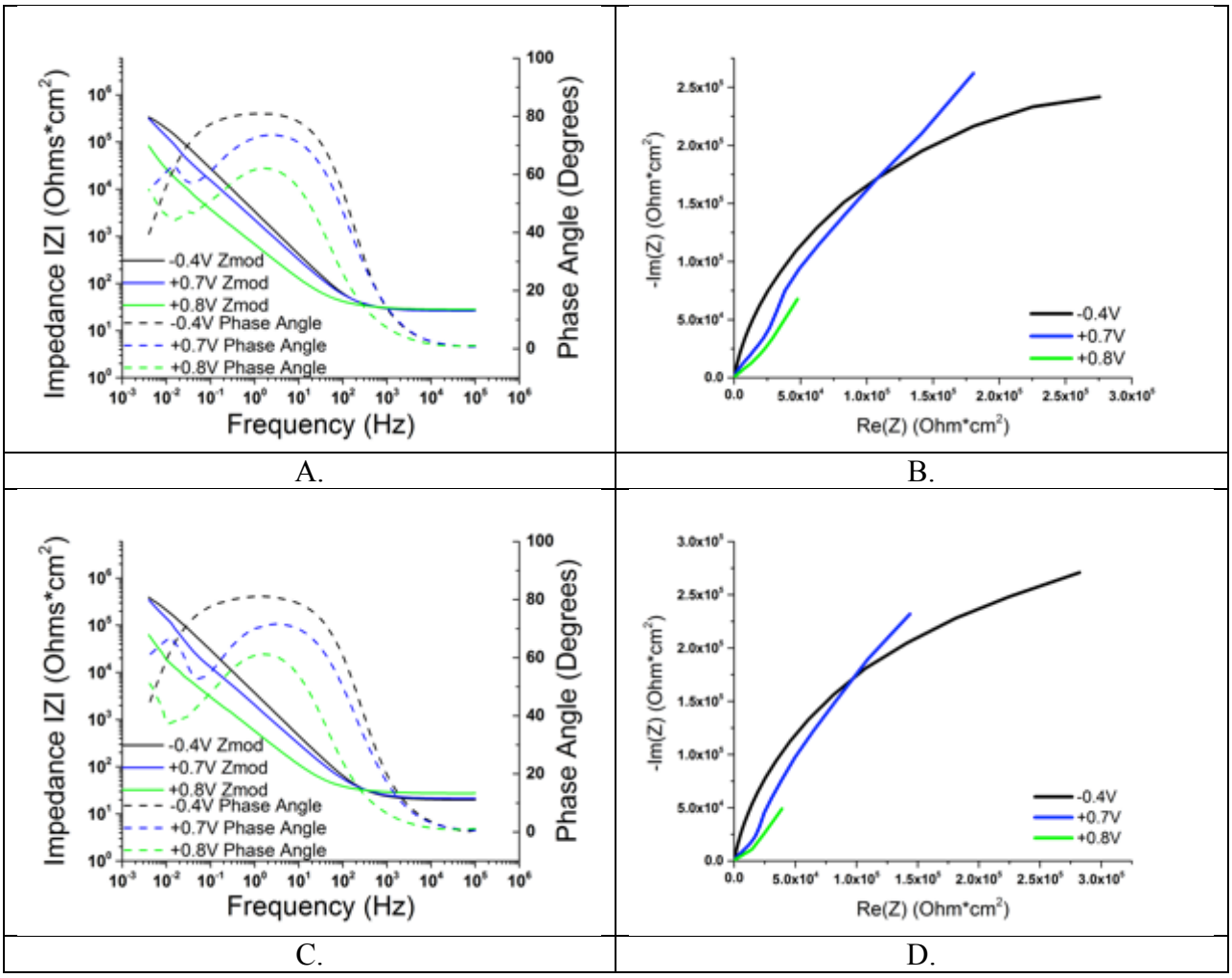

Figure 4.2. Bode and Nyquist Plots (A) Bode Plot After Treatment using 8 mM of SMD, (B) Nyquist Plot After Treatment using 8 mM of SMD, (C) Bode Plot After Treatment using 32 mM SMD, and (D) Nyquist Plot After Treatment using 32 mM SMD.

In order to quantify the resistance and capacitance of the additive, an equivalent circuit was used shown in Figure 2.7B in Part 1. Additionally, Chi-squared were in an acceptable range allowing this circuit to exemplify the condition of the cell. The resistance after treatment for both concentrations of SMD is given in Figure 4.3A. In both 8 mM and 32 mM of SMD, +0.8 V results in the lowest resistance after treatment than the -0.4 V and the +0.7 V treatment potentials. However, in either concentration of the additive, +0.7 V resulted in the highest resistance after treatment. The capacitance after treatment for each potential treatment in 8 mM

and 32 mM SMD is shown in Figure 4.3B. In both concentrations of the additive, +0.8 V shows the highest capacitance, which is proportional to corrosion. -0.4 V and +0.7 V resulted in lower capacitance after treatment values compared to +0.8 V. In Figure 4.3C which shows the ratio of the resistance after treatment over resistance before treatment for each of the treatment potentials indicates that +0.7 V as the treatment potential outcomes in largest ratio when SMD concentration increased. Additionally, this potential treatment with 32 mM SMD, outcomes in a lower ratio of capacitance, showed in Figure 4.3D.

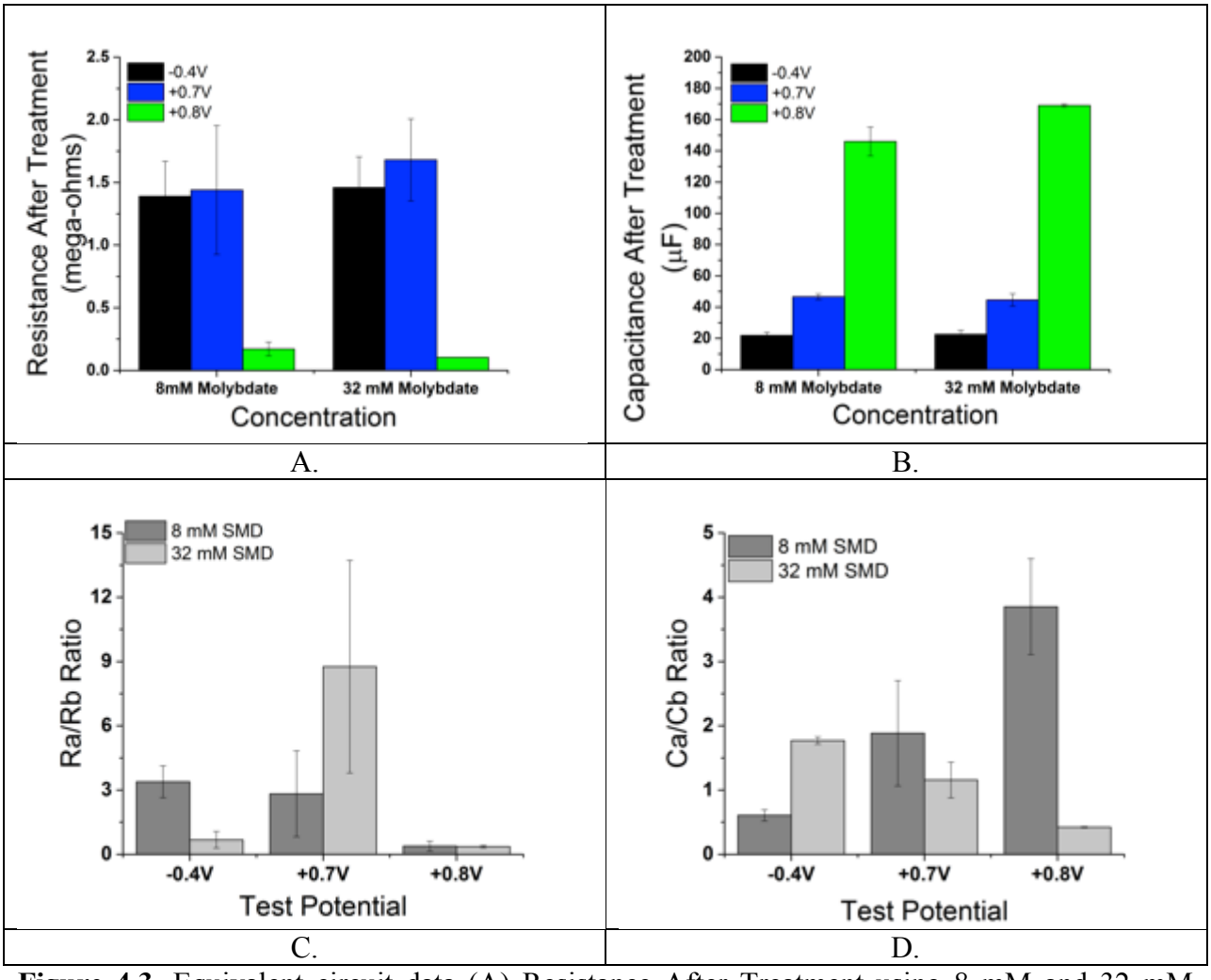

Figure 4.3. Equivalent circuit data (A) Resistance After Treatment using 8 mM and 32 mM SMD, (B) Capacitance After Treatment using 8 mM and 32 mM SMD, (C) Ratio of Resistance After Treatment over Resistance Before Treatment, and (D) Ratio of Capacitance After Treatment to Capacitance After Treatment using treatment potentials of -0.4 V, +0.7 V and +0.8 V.

The WLI images and surface roughness are shown in Figure 4.4A-F. The highest surface roughness is displayed by the +0.8 V potential in regards to either SMD concentration. This may help to verify that this potential undergoes more corrosion (Figure 4.3A and 4.3B) since the surface roughness is higher. Based on concentrations of the additive, 32 mM of SMD outcomes in lower surface roughness than 8 mM of SMD. This may be attributed to the binding properties and affinity of molybdenum, which would result in a lower surface roughness. Overall, the treatment condition that resulted in the lowest surface roughness was the +0.7 V treatment potential in 30 g/L protein content with 32 mM of SMD.

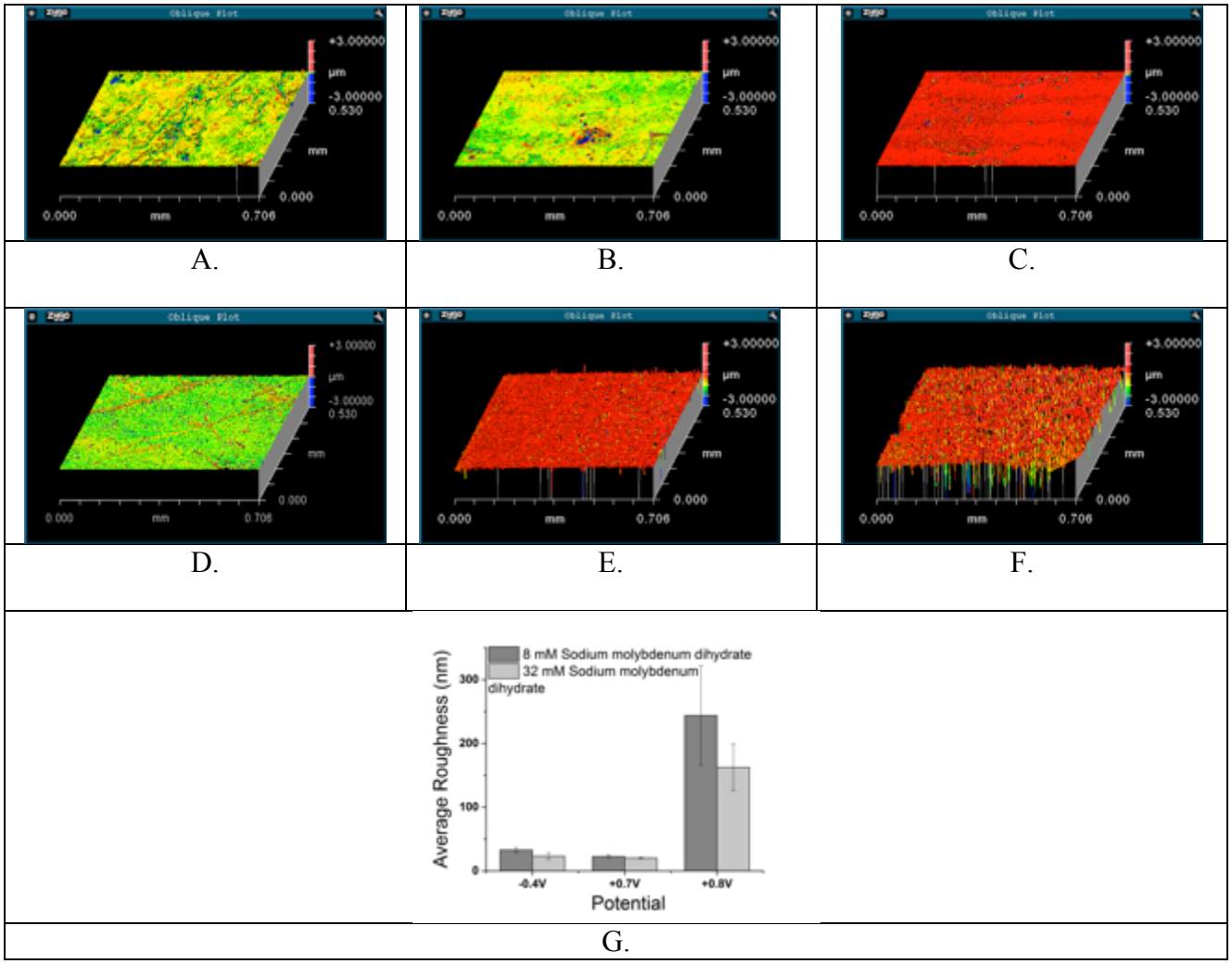

Figure 4.4. White light interferometry (A) -0.4 V in 30 g/L protein content with 8 mM of SMD, (B) -0.4 V in 30 g/L protein content with 32 mM of SMD, (C) +0.7 V in 30 g/L protein content with 8 mM SMD, (D) +0.7 V in 30 g/L protein content with 32 mM SMD, (E) +0.8 V in 30 g/L protein content with 8 mM SMD, (F) +0.8 V in 30 g/L protein content with 32 mM SMD, (G) Average roughness (nm) of samples using SMD.

The SEM images using SMD are shown in Figure 4.5A-F. A thicker film appears in all the darker colored portions of each image. After conducting EDS on these locations it was confirmed that more homogenous, even layers of this film had normal molybdenum amounts, however more concentrated regions of the film resulted in higher amounts of molybdenum content. Increasing SMD content from 8 mM to 32 mM for each potential resulted in SEM images that had more of an even and homogenous film layer.

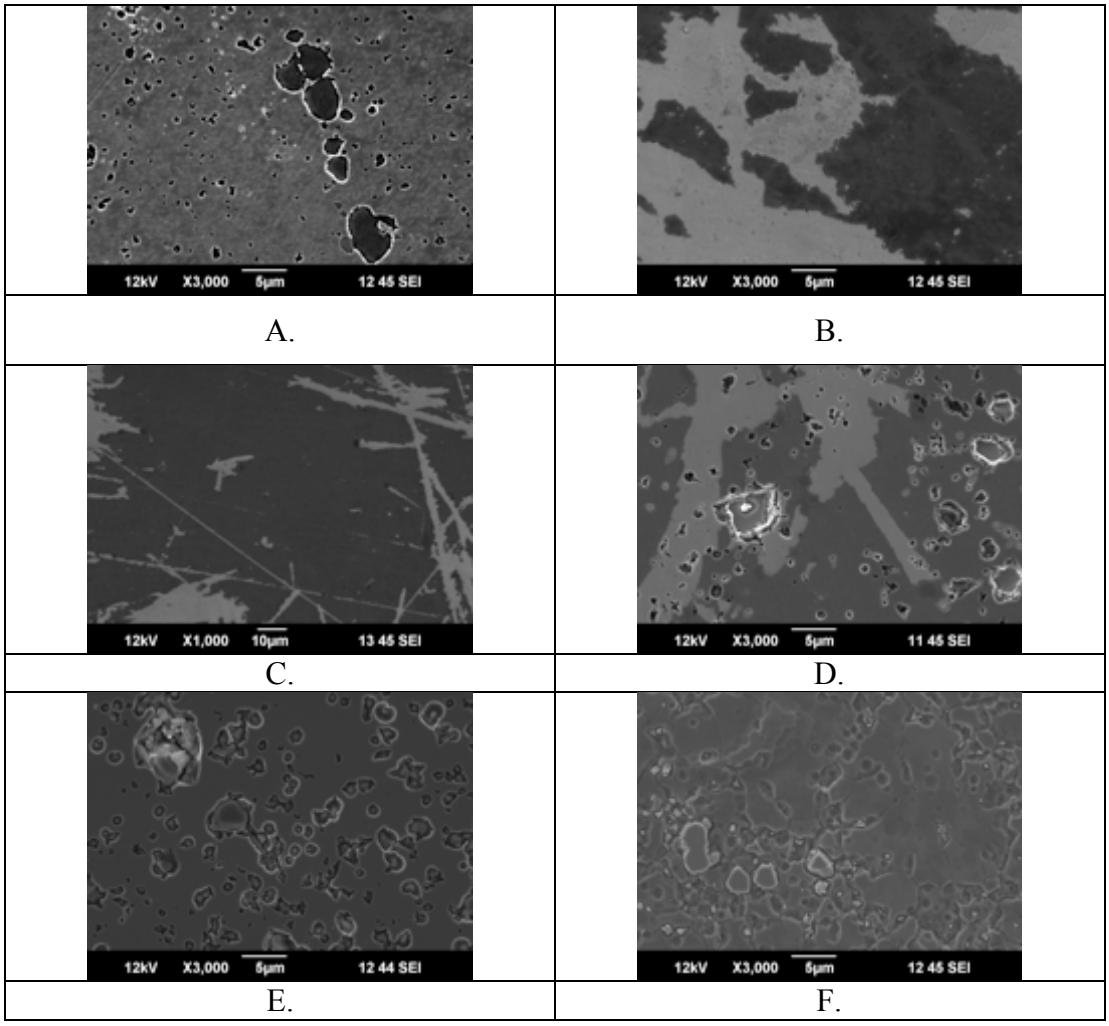

Figure 4.5 Scanning electron microscopy (A) -0.4 V in 30 g/L protein content with 8 mM SMD, (B) -0.4 V in 30 g/L protein content with 32 mM SMD, (C) +0.7 V in 30 g/L protein content with 8 mM SMD, (D) +0.7 V in 30 g/L protein content with 32 mM SMD, (E) +0.8 V in 30 g/L protein content with 8 mM SMD, and (F) +0.8 V in 30 g/L protein content with 32 mM SMD.

4.4 Discussion

When comparing the resistance after treatment of both concentrations of the additive, it can be seen in Figure 4.3A that there is no significant difference between each corresponding treatment potential in either concentration. Therefore, it appears that higher concentration of SMD at least from a concentration increase of 8 mM to 32 mM does not appear to affect corrosion resistance. Similarly, when taking a look at Figure 4.3B, which displays the capacitance after treatment under the two concentrations of SMD, the capacitance is close in

value to either additive concentration. This leads to determining that the increase of the additive 4-fold from 8 mM to 32 mM was not enough to cause a significant change in the resistance and capacitance values after the treatment step. Therefore, it would be helpful to include larger concentrations of SMD in the electrolyte and observe and measure any changes in resistance and capacitance values. However, there may be a specific concentration less than 8 mM of the additive, which serves as the peak concentration. This means that after this concentration of the additive there would be a steady resistance and capacitance value for any concentration higher than the peak concentration. Therefore, the values displayed using 8 mM and 32 mM may have been after that specific peak concentration and only subtle changes in the resistance and capacitance was observed. After EDS analysis under SEM (Figure 4.5), it was observed that higher concentrations of SMD resulted in more homogenous, even film with lower molybdenum content. This was in comparison to the 8 mM of SMD that resulted in more concentrated, smaller regions with higher molybdenum content. In Figure 4.5A and B, which show -0.4 V with 8 mM and 32 mM SMD, respectively, indicates this potential outcomes is more homogenous film with increasing SMD concentration. The same is also seen with +0.7 V in Figure 4.5C and D. This indicates increasing molybdenum has an effect of providing a more uniform film. Therefore, it appears as though higher molybdenum concentration outcomes in more even film formation with normal molybdenum content than lower concentrations of SMD, which resulted in spotted, smaller, and higher molybdenum-rich regions.

In Figure 4.6, a schematic diagram of the treatment potentials in 30 g/L protein content in either SMD concentration is shown. In Figure 4.6A, which shows the -0.4 V potential treatment, does not appear to have any electrochemically treated film as the SEM images of this potential did not result in surface film formation, this was also verified by EDS which did not report the

presence carbonaceous film. In Figure 4.6B, showing the +0.7 V potential treatment results in film formation appeared, which was verified by EDS. The difference is that this potential may have caused a higher rate of metal ion release, as this potential results in greater current density (Figure 2.1). This may be a key process since more metal ions would be responsible for increased bonding to occur to form the film. Lastly, the potential treatment of +0.8 V is shown in Figure 4.6C. This potential outcomes in a thinner film since too many metal ions have been released from the alloy as verified by Figure 2.1. This would cause a decrease in film formation since the metal ions are incorporated into the surrounding electrolyte and not close to the alloy surface. Additionally, it was evaluated that +0.8 V outcomes in the lowest R_p and the highest capacitance.

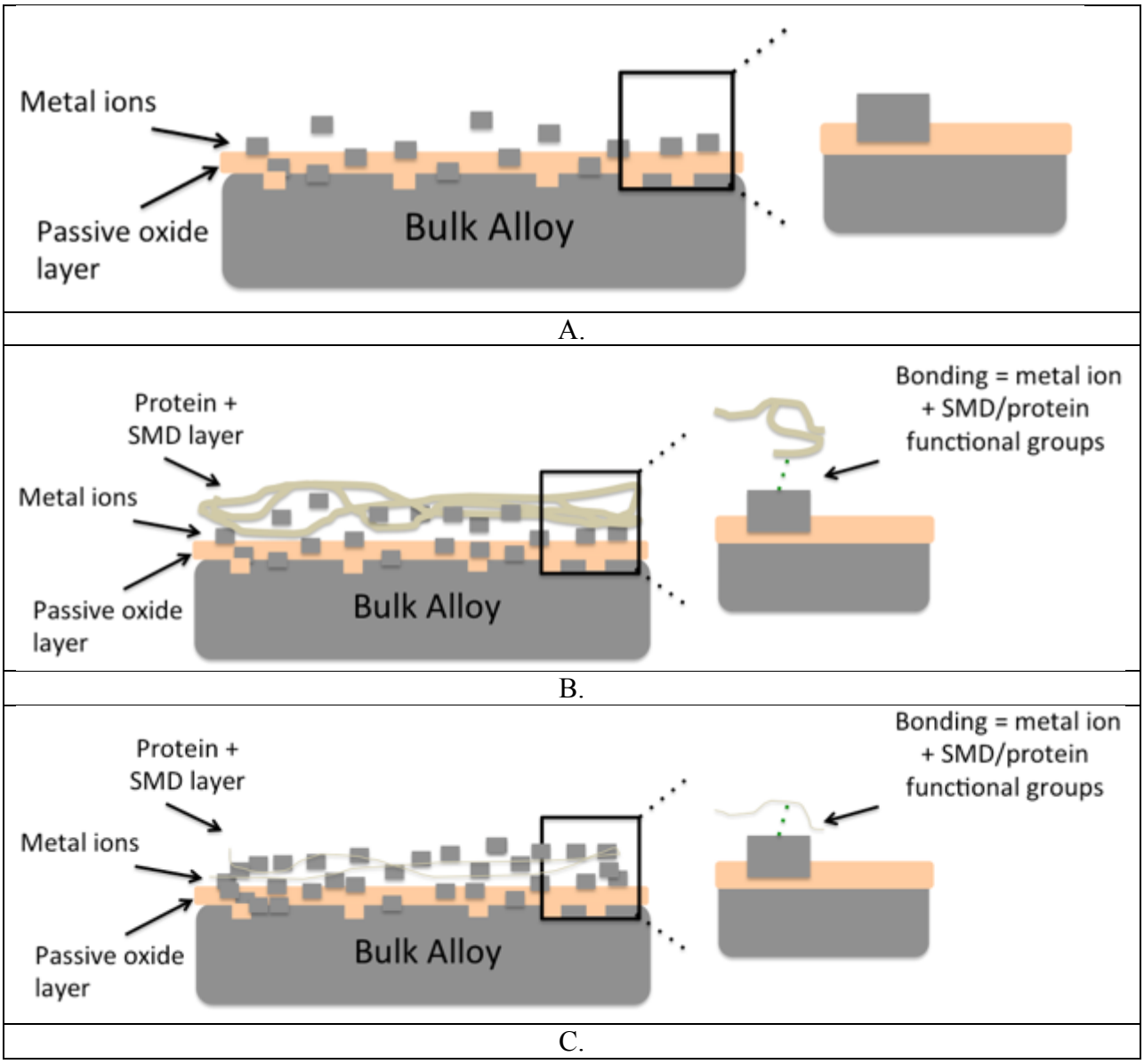

Figure 4.6. Proposed mechanism of Part 3 (A) -0.4 V, (B) +0.7 V, and (C) +0.8 V.

4.5 Conclusion

The next step includes conducting tribocorrosion testing on these samples using similar parameters during Part 2. Conducting these experiments will help to determine any effects of incorporating molybdate additives in surrounding media to understand the role of molybdenum in film integrity and film durability during mechanical testing. Lastly, it would be beneficial to

determine the thickness of the film in each condition. From Part 3, the following conclusions can be drawn:

1. In both 8 mM and 32 mM concentrations of SMD, +0.7 V displayed superior corrosion kinetics than any other potential treatment (-0.4 V or +0.8 V).

2. Increasing SMD concentration from 8 mM to 32 mM did not significantly increase the R_p. However, there was a slight increase seen with increasing concentration.

3. SEM images indicate that with increasing SMD concentration, film appearance is more homogeneous and even compared with lower SMD concentration using potentials of +0.7 V and +0.8 V.

5. Sodium Molybdate Dihydrate Deposition through UV Light: A Comparison Between Treatment Methods (Part 4)

5.1 Introduction

Exposure of UV Light is able to create crosslinking (covalent bonds) between protein complexes and DNA [38]. Therefore, by exposing the treated film in phosphate buffered saline (PBS) with 8 mM of sodium molybdate dihydrate (SMD) under UV light (24 hrs.) there might be a increasing in the bonding between the protein and additive, as UV light is able to create crosslinking. Although, in the present study, protein-metal ions are to be bonded and not protein-DNA interactions, the former condition was evaluated using electrochemical techniques.

In order to determine how the bonding mechanism of SMD affects corrosion kinetics, a new treatment method was carried out. An introduction of a new treated group with +0.7 V in 30 g/L protein content was used, which was then soaked in phosphate buffered saline (PBS) with 8 mM of SMD. This group was created in order to determine how layered SMD deposition affects corrosion kinetics. A comparison was made between treatments of a CoCrMo alloy disc (control), a CoCrMo alloy disc that was soaked in PBS with 8 mM SMD under 24 hrs. of UV light, a treatment condition of +0.7 V in 30 g/L protein content, +0.7 V in 30 g/L protein content with 8 mM SMD, and a previously treated film using +0.7 V in 30 g/L protein content the soaked in PBS with 8 mM SMD with SMD under 24 hrs. of UV light. Each of these conditions was then placed under electrochemical testing. Electrochemical testing consisted of open circuit potential (OCP) tests and electrochemical impedance spectroscopy (EIS) tests to determine surface properties.

5.2 Materials and Methods

Sample preparation: A control CoCrMo alloy disc was prepared to an Ra < 15.0 nm. Previously treated samples using conditions of +0.7 V in 30 g/L protein content (Part 1) and +0.7 V in 30 g/L protein content with 8 mM of SMD (Part 3) were investigated. Additionally, a new

group of +0.7 V in 30 g/L protein content samples was prepared under the protocol given in Part 1. This group was then exposed to PBS with 8 mM of SMD for 24 hrs. under UV light, in order to create a layered effect (SMD on top of the proteinaceous film). A CoCrMo alloy disc (Ra < 15.0 nm) was also placed in PBS with 8 mM of SMD for 24 hrs. under UV light. After UV light exposure, the samples were sonicated for 20 minutes in distilled water. The treatment conditions are seen Figure 5.1.

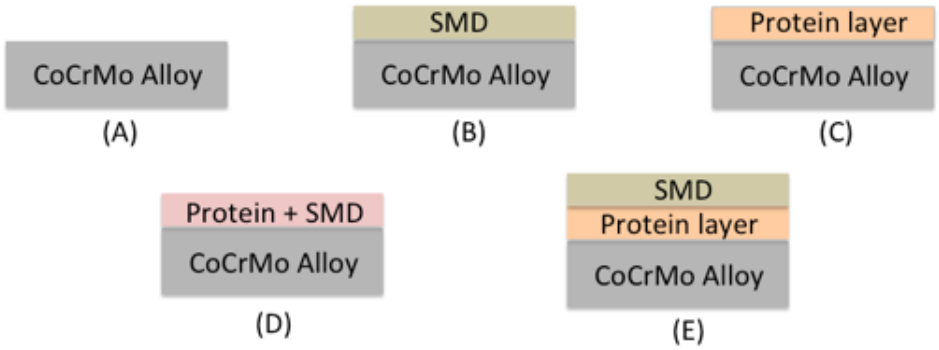

Figure 5.1. Treatment conditions (A) CoCrMo Alloy (control), (B) CoCrMo Alloy, UV treated (24 hrs.) in PBS with 8 mM SMD, (C) +0.7 V in 30 g/L protein content, (D) +0.7 V in 30 g/L protein content with 8 mM SMD, (E) CoCrMo Alloy treated at +0.7 V in 30 g/L protein content, then UV treated (24 hrs.) in PBS with 8 mM SMD.

Electrochemical testing: Electrochemical testing was conducted using a standard three-electrode corrosion cell (Figure 2.2). The CoCrMo alloy discs were used as the working electrodes (WE) and each disc had 0.38 cm^2 of exposed surface area in the corrosion well. The other two electrodes were a graphite rod counter electrode and a reference electrode, which was a saturated calomel electrode (SCE). A quantity of 10 mL of 30 g/L protein content electrolyte was used for each sample and was warmed to 37 °C. All tests were maintained at the physiological temperature of 37 °C using a water bath during the electrochemical testing.

The testing protocol consisted of a total of four electrochemical tests. The first test was an OCP of 3 min, which was done to check all electrical connections. The second test was another OCP, but for 10 min, which allowed for the sample to stabilize in the specific conditions of the

cell. The third test was an EIS test, which measured the surface properties of the sample after their specific conditions. EIS testing (at E_{oc}, potential amplitude: ±10 mV, frequency range: 100 KHz-0.005 Hz) was done to measure the properties of the material surface after the application of the treatment condition. The last test, which is also an OCP, measured if there was a change in the potential based on the treatment.

After each experiment the electrolyte was taken out and stored properly, the WE sample was removed and sonicated again using the same cleaning protocol as before the experiment: sonicated for 20 minutes using distilled water.

5.3 Results

In order to quantify the corrosion kinetics of these samples, Nyquist and Bode plots were made. The Bode plot is shown in Figure 5.2A and the Nyquist plot is shown in Figure 5.2B. Based on the Bode plot in Figure 5.2A, the treatment condition which displays superior film formation properties is the UV treated sample which was first treated to +0.7 V in 30 g/L protein content then placed in PBS with 8 mM SMD (24 hrs.). There are two time constants shown with the untreated UV sample which was exposed to +0.7 V in 30 g/L protein content with 8 mM SMD at the same time. It is the only condition which outcomes in two time constants throughout the frequency spectrum. In Figure 5.2B, the Nyquist plot shows the condition which outcomes in superior corrosion kinetics is the sample that was untreated with +0.7 V in 30 g/L protein content. Secondly, it appears as though the two conditions which have similar Nyquist plots are the untreated +0.7 V in 30 g/L protein content condition and the condition that was first subjected to film formation at +0.7 V in 30 g/L protein content then UV treated in PBS with 8 mM SMD (24 hrs.). However, based on the two methods for exposing the bulk alloy to SMD, it appears as though the superior treatment is the UV treated samples compared to the method in Part 3 which was incorporating 8 mM SMD into the electrolyte of 30 g/L protein content. The

polarization resistance and the capacitance of Groups D and E are shown in Figure 5.2C and 5.2D, respectively. These values were quantified using the same equivalent circuit in Figure 2.6. The UV treated (T-UV) group has a higher polarization resistance than the group that was un-treated (UT). In addition the treated group (T-UV) has a lower capacitance than the untreated group. The only change between these groups is the way that SMD was applied. Therefore, it is seen that UV treatment of SMD outcomes in a film that is able to lower the tendency of corrosion as indicated by the higher polarization resistance and lower capacitance.

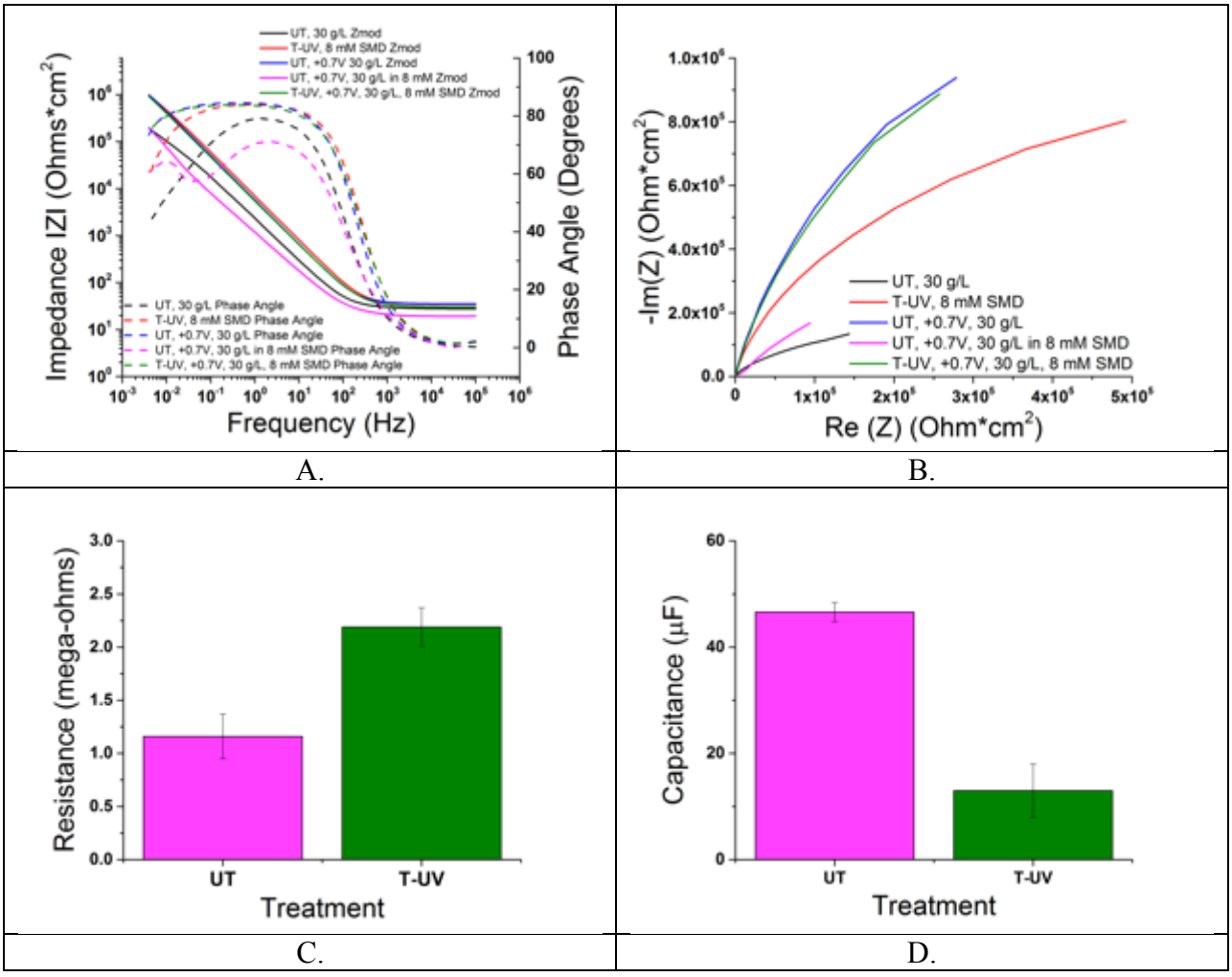

Figure 5.2. Electrochemical impedance spectroscopy data (A) Bode plots, (B) Nyquist plots, (C) Resistance of SMD treatment methods, and (D) Capacitance of SMD treatment methods.

5.4 Discussion

The EIS results have demonstrated that film previously treated at +0.7 V in 30 g/L protein content and then exposed to UV treatment using 8 mM SMD in PBS appears to display superior corrosion kinetics compared to the treatment condition of +0.7 V in 30 g/L protein content with 8 mM SMD. It is believed that the UV treatment is able to help with creating bonding between proteinaceous layer mixed with metal ions and the UV deposited 8 mM SMD layer.

Specifically, the bonding between the proteinaceous film treated at +0.7 V in 30 g/L protein content and the UV deposited PBS with 8 mM SMD layer occurs through chemisorption, which allows for a material to adhere to a surface. Through chemisorption, self-assembled monolayers (SAMs) are created of the molybdate [MoO_4^{2-}] anions. In Figure 5.4, the interaction between the +0.7 V in 30 g/L protein content film and molybdate anions is shown. It is possible that the molybdate anions were able to structure into SAMs onto the proteinaceous film since UV light was able to facilitate bonding between the film and the molybdate anions.

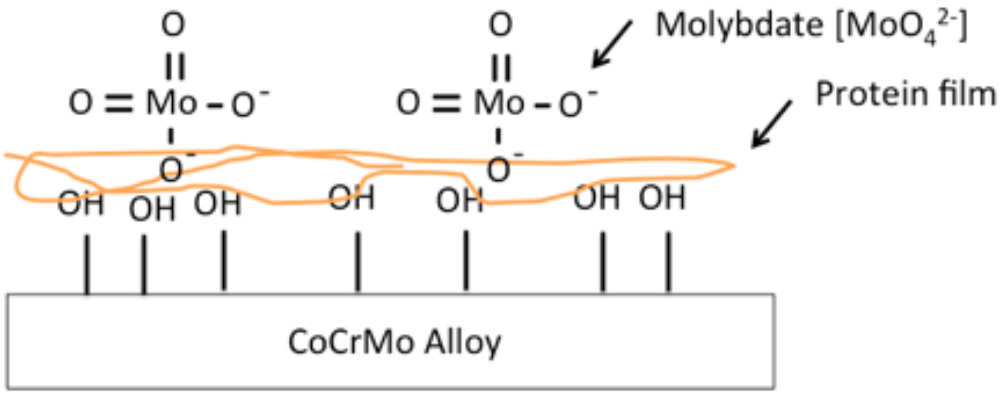

Figure 5.4. Proposed mechanism of Part 4. Molybdate ions are able to bond to electrochemically treated film.

5.5 Conclusion

The next step for this part of the study includes conducting tribocorrosion tests using similar parameters during Part 2. Conducting these experiments will help to determine any affects of UV treatment of SMD. It would be interesting to quantify the thickness of the film for each condition investigated as well in order to quantify the thickness of the molybdate anions adhering to the protein film. From Part 4, the following conclusions can be drawn:

1. UV treatment of samples in PBS with 8 mM SMD for 24 hrs. resulted in superior corrosion kinetics than samples that were treated with an electrolyte of 30 g/L protein content with 8 mM SMD.

6. Encompassing Discussion

Based on the results of Part 1 and Part 3 film formation is resultant of interactions between the bulk alloy surface and the surrounding electrolyte occurring at the treatment potentials. +0.7 V with 30 g/L protein content was a treatment condition of key interest, since previous findings have indicated an applied potential of +0.77 V results in a proteinaceous film formation on CoCrMo films and show evidence of $Mo^{(+6)}$ ions assisting in initiating film formation processes [30]. The treatment potentials were able to induce CoCrMo corrosion in the form of pits and grain boundary corrosion, resulting in metal ion exposure at the alloy surface which may allow for bonding interactions to occur between the alloy and electrolyte using treatments of +0.7 V and +0.8 V in a proteinaceous electrolyte. Because of these interactions due to environmental and mechanical factors, the strongest film resistant to mechanical movement in Part 2 during tribocorrosion testing was the +0.7 V in 30 g/L protein content condition. Surface characterization techniques also supported this condition as superior than other conditions.

We believe that $Mo^{(+6)}$ ions are able to bond to particular amino acids within albumin. However, the specific of bonding is still not known yet. To address why the potential of +0.7 V outcomes in a superior surface treatment is still under question. However, we speculate that the potentiostatic treatment of +0.7 V which is in the transpassive region of CoCrMo alloy outcomes in anodic corrosion of this particular alloy to generate an ideal metal ion release rate ideal for proteinaceous film formation to occur. There was also strong evidence that increases in molybdate concentration through SMD revealed that under SEM imaging, the film became more homogenous in appearance.

7. Encompassing Conclusion

7.1 Clinical Scope

Understanding the corrosion and wear mechanisms of hip joint implants will help to guide future design and functional needs of implants. Biological response to metal debris is an area for pressing concern; urgent attention is needed to deter the effects of MoM wear and corrosion. In addition, this investigation adds to the knowledge of how proteins in the synovial fluid affect corrosion kinetics of implants and understanding the role of film formation to provide protection to implant surfaces during *in vivo* mechanical loading conditions.

7.2 Project Outlook

Although this study has shown that film formation may be able to limit CoCrMo alloy corrosion and help lower friction during articulation, further studies are still needed. Other parameters to investigate include protein content (concentration), pH levels of surrounding electrolyte, loading/number of cycles during tribocorrosion testing, and other additives to understand the role of film formation in implant corrosion. These studies will utilize the experience and expertise of engineers (i.e. biomedical, chemical, mechanical, corrosion), tribologists, and orthopedic surgeons to help understand implant longevity and survivorship.

8. References

[1] B. Nwachukwu, K. Bozic, W. Schairer, J. Bernstein, D. Jevsevar, R. Marx, and D. Padgett, "Current Status of Cost Utility Analyses in Total Joint Arthroplasty: A Systematic Review," *Clin Orthop Relat Res*, pp. 1–13, Sep. 2014.

[2] C. Wyles, J. Jimenez-Almonte, M. Murad, G. Norambuena-Morales, M. Cabanela, R. Sierra, and R. Trousdale, "There Are No Differences in Short- to Mid-term Survivorship Among Total Hip-bearing Surface Options: A Network Meta-analysis," *Clin Orthop Relat Res*, pp. 1–11, Dec. 2014.

[3] S. Kurtz, K. Ong, E. Lau, F. Mowat, and M. Halpern, "Projections of Primary and Revision Hip and Knee Arthroplasty in the United States from 2005 to 2030," *The Journal of Bone & Joint Surgery*, vol. 89, no. 4, pp. 780–785, Apr. 2007.

[4] G. Perino, B. Ricciardi, S. Jerabek, G. Martignoni, G. Wilner, D. Maass, S. Goldring, and P. Purdue, "Implant based differences in adverse local tissue reaction in failed total hip arthroplasties: a morphological and immunohistochemical study," *BMC Clinical Pathology*, vol. 14, no. 1, p. 39, 2014.

[5] V. Shetty, B. Shitole, G. Shetty, H. Thakur, and M. Bhandari, "Optimal bearing surfaces for total hip replacement in the young patient: a meta-analysis," *International Orthopaedics (SICOT)*, vol. 35, no. 9, pp. 1281–1287, Sep. 2011.

[6] I. Catelas and M. A. Wimmer, "New Insights into Wear and Biological Effects of Metal-on-Metal Bearings," *The Journal of Bone & Joint Surgery*, vol. 93, no. Supplement 2, pp. 76–83, May 2011.

[7] D. Berry, M. Abdel, and J. Callaghan, "What Are the Current Clinical Issues in Wear and Tribocorrosion?," *Clin Orthop Relat Res*, pp. 1–6, Apr. 2014.

[8] M. Mathew, J. Jacobs, and M. Wimmer, "Wear-Corrosion Synergism in a CoCrMo Hip Bearing Alloy Is Influenced by Proteins," *Clin Orthop Relat Res*, vol. 470, no. 11, pp. 3109–3117, Nov. 2012.

[9] J. J. Jacobs, R. M. Urban, N. J. Hallab, A. K. Skipor, A. Fischer, and M. A. Wimmer, "Metal-on-metal Bearing Surfaces," *Journal of the American Academy of Orthopaedic Surgeons*, vol. 17, no. 2, pp. 69–76, Feb. 2009.

[10] J. Hesketh, M. Ward, D. Dowson, and A. Neville, "The composition of tribofilms produced on metal-on-metal hip bearings," *Biomaterials*, vol. 35, no. 7, pp. 2113–2119, Feb. 2014.

[11] D. Dowson, "New joints for the Millennium: Wear control in total replacement hip joints," *Proceedings of the Institution of Mechanical Engineers, Part H: Journal of Engineering in Medicine*, vol. 215, no. 4, pp. 335–358, Apr. 2001.

[12] A. Lombardi Jr, K. Berend, M. Morris, J. Adams, and M. Sneller, "Large-diameter Metal-on-metal Total Hip Arthroplasty: Dislocation Infrequent but Survivorship Poor," *Clin Orthop Relat Res*, pp. 1–12, Nov. 2014.

[13] I. Catelas, J. D. Bobyn, J. B. Medley, J. J. Krygier, D. J. Zukor, and O. L. Huk, "Size, shape, and composition of wear particles from metal–metal hip simulator testing: Effects of alloy and number of loading cycles," *J. Biomed. Mater. Res.*, vol. 67A, no. 1, pp. 312–327, 2003.

[14] M. Scaglione, L. Fabbri, N. Bianchi, D. Dell'Omo, and G. Guido, "Metal-on-metal hip resurfacing: correlation between clinical and radiological assessment, metal ions and ultrasound findings," *Musculoskelet Surg*, pp. 1–9, Dec. 2014.

[15] H.-G. Willert, G. H. Buchhorn, A. Fayyazi, R. Flury, M. Windler, G. Köster, and C. H. Lohmann, "Metal-on-Metal Bearings and Hypersensitivity in Patients with Artificial Hip Joints," *The Journal of Bone & Joint Surgery*, vol. 87, no. 1, pp. 28–36, Jan. 2005.

[16] O. M. Posada, R. J. Tate, and M. H. Grant, "Effects of CoCr metal wear debris generated from metal-on-metal hip implants and Co ions on human monocyte-like U937 cells," *Toxicology in Vitro*, vol. 29, no. 2, pp. 271–280, Mar. 2015.

[17] P. Campbell, M. Kung, A. Hsu, and J. Jacobs, "Do Retrieval Analysis and Blood Metal Measurements Contribute to Our Understanding of Adverse Local Tissue Reactions?," *Clin Orthop Relat Res*, vol. 472, no. 12, pp. 3718–3727, Dec. 2014.

[18] S. Almousa, N. Greidanus, B. Masri, C. Duncan, and D. Garbuz, "The Natural History of Inflammatory Pseudotumors in Asymptomatic Patients After Metal-on-metal Hip Arthroplasty," *Clin Orthop Relat Res*, vol. 471, no. 12, pp. 3814–3821, Dec. 2013.

[19] Y.-M. Kwon, S. J. Ostlere, P. McLardy-Smith, N. A. Athanasou, H. S. Gill, and D. W. Murray, "'Asymptomatic' Pseudotumors After Metal-on-Metal Hip Resurfacing Arthroplasty: Prevalence and Metal Ion Study," *The Journal of Arthroplasty*, vol. 26, no. 4, pp. 511–518, Jun. 2011.

[20] Y. Liao, E. Hoffman, M. Wimmer, A. Fischer, J. Jacobs, and L. Marks, "CoCrMo Metal-on-Metal Hip Replacements," *Physical chemistry chemical physics : PCCP*, vol. 15, no. 3, p. 10.1039/c2cp42968c, Jan. 2013.

[21] J. Ø. Penny, J. Varmarken, O. Ovesen, C. Nielsen, and S. Overgaard, "Metal ion levels and lymphocyte counts: ASR hip resurfacing prosthesis vs. standard THA: 2–year results from a randomized study," *Acta Orthopaedica*, vol. 84, no. 2, pp. 130–137, Dec. 2012.

[22] G. A. Afolaranmi, M. Akbar, J. Brewer, and M. H. Grant, "Distribution of metal released from cobalt–chromium alloy orthopaedic wear particles implanted into air pouches in mice," *J. Biomed. Mater. Res.*, vol. 100A, no. 6, pp. 1529–1538, 2012.

[23] N. Diomidis, S. Mischler, N. S. More, and M. Roy, "Tribo-electrochemical characterization of metallic biomaterials for total joint replacement," *Acta Biomaterialia*, vol. 8, no. 2, pp. 852–859, Feb. 2012.

[24] M. P. Souza, L. Lima, C. P. Lima, C. C. Zavaglia, and C. A. Freire, "Effects of pH on the electrochemical behaviour of titanium alloys for implant applications," *J Mater Sci: Mater Med*, vol. 20, no. 2, pp. 549–552, Feb. 2009.

[25] B. Shahgaldi, F. Heatley, A. Dewar, and B. Corrin, "In vivo corrosion of cobalt-chromium and titanium wear particles," *Journal of Bone & Joint Surgery, British Volume*, vol. 77-B, no. 6, pp. 962–966, Nov. 1995.

[26] M. T. Mathew, C. Nagelli, R. Pourzal, A. Fischer, M. P. Laurent, J. J. Jacobs, and M. A. Wimmer, "Tribolayer formation in a metal-on-metal (MoM) hip joint: An electrochemical investigation," *Journal of the Mechanical Behavior of Biomedical Materials*, vol. 29, no. 0, pp. 199–212, Jan. 2014.

[27] M. A. Wimmer, C. Sprecher, R. Hauert, G. Täger, and A. Fischer, "Tribochemical reaction on metal-on-metal hip joint bearings: A comparison between in-vitro and in-vivo results," *Wear*, vol. 255, no. 7–12, pp. 1007–1014, Aug. 2003.

[28] M. A. Wimmer, A. Fischer, R. Büscher, R. Pourzal, C. Sprecher, R. Hauert, and J. J. Jacobs, "Wear mechanisms in metal-on-metal bearings: The importance of tribochemical reaction layers," *J. Orthop. Res.*, vol. 28, no. 4, pp. 436–443, 2010.

[29] Y. Liao, R. Pourzal, M. A. Wimmer, J. J. Jacobs, A. Fischer, and L. D. Marks, "Graphitic Tribological Layers in Metal-on-Metal Hip Replacements," *Science*, vol. 334, no. 6063, pp. 1687–1690, Dec. 2011.

[30] E. J. Martin, R. Pourzal, M. T. Mathew, and K. R. Shull, "Dominant Role of Molybdenum in the Electrochemical Deposition of Biological Macromolecules on Metallic Surfaces," *Langmuir*, vol. 29, no. 15, pp. 4813–4822, Apr. 2013.

[31] R. Kuprienko, "Does Protein Content of the Surrounding Body Fluid Influence the Corrosion Resistance of the CoCrMo alloy in a Hip Prosthesis?," presented at the ORS 2013 Annual Meeting, 2013.

[32] L. E. Guenther, B. W. Pyle, T. R. Turgeon, E. R. Bohm, U. P. Wyss, T. A. Schmidt, and J.-M. Brandt, "Biochemical analyses of human osteoarthritic and periprosthetic synovial fluid," *Proceedings of the Institution of Mechanical Engineers, Part H: Journal of Engineering in Medicine*, vol. 228, no. 2, pp. 127–139, Feb. 2014.

[33] Y. Liao, E. Hoffman, M. Wimmer, A. Fischer, J. Jacobs, and L. Marks, "CoCrMo metal-on-metal hip replacements," *Phys. Chem. Chem. Phys.*, vol. 15, no. 3, pp. 746–756, 2013.

[34] C. Myant and P. Cann, "On the matter of synovial fluid lubrication: Implications for Metal-on-Metal hip tribology," *Journal of the Mechanical Behavior of Biomedical Materials*, vol. 34, no. 0, pp. 338–348, Jun. 2014.

[35] V. Swaminathan and J. L. Gilbert, "Fretting corrosion of CoCrMo and Ti6Al4V interfaces," *Biomaterials*, vol. 33, no. 22, pp. 5487–5503, Aug. 2012.

[36] A. Igual Muñoz and S. Mischler, "Effect of the environment on wear ranking and corrosion of biomedical CoCrMo alloys," *J Mater Sci: Mater Med*, vol. 22, no. 3, pp. 437–450, Mar. 2011.

[37] J. L. Gilbert, S. Mali, R. M. Urban, C. D. Silverton, and J. J. Jacobs, "In vivo oxide-induced stress corrosion cracking of Ti-6Al-4V in a neck–stem modular taper: Emergent behavior in a new mechanism of in vivo corrosion," *J. Biomed. Mater. Res.*, vol. 100B, no. 2, pp. 584–594, 2012.

[38] L. A. Chodosh, "UV Crosslinking of Proteins to Nucleic Acids," in *Current Protocols in Molecular Biology*, John Wiley & Sons, Inc., 2001.

APPENDIX

Shelley Kerwell
Skerwe2@uic.edu

March 12th, 2015

Dear Dr. M. T. Mathew:

I am writing to request permission to use the Potentiodynamic Curve from your poster:

R. Kuprienko, "Does Protein Content of the Surrounding Body Fluid Influence the Corrosion Resistance of the CoCrMo alloy in a Hip Prosthesis?," presented at the ORS 2013 Annual Meeting, 2013.

in my thesis, as you are the Corresponding Author. This material will appear as originally published with the transpassive potentials and the reference potential displayed. Unless you request otherwise, I will use the conventional style of the Graduate College of the University of Illinois at Chicago as acknowledgment.

A copy of this letter is included for your records. Thank you for your kind consideration of this request.

Sincerely,

Shelley Kerwell

The above request is approved.

Approved by: M Mathew Date: 03/12/2015

M T Mathew, PhD
Assistant Professor
Dept. of Orthopedics
Rush University
Chicago - IL

VITA

NAME: Shelley Kerwell

EDUCATION: B.S., Bioengineering, University of Illinois at Chicago, Illinois, 2013
M.S., Bioengineering, University of Illinois at Chicago, Illinois, 2015

PROFESSIONAL MEMBERSHIP: Alpha Eta Mu Beta
Tau Beta Pi

ABSTRACTS: Kerwell, S., Baer, D., Martin, E., Wimmer, M., Shull, K., Mathew, M. T.: Electrochemically Treated Proteinaceous Film Formation on CoCrMo Alloy for Hip Prostheses, Orthopedic Research Society, 2015.

Kerwell, S., Alfaro, M., Pourzal, R., Mercuri, L. G., Sukotjo, C., Mathew, M. T.: Investigation on the Failure Mechanisms of Retrieved Temporomandibular Joint Implants: A Bioengineering Perspective. TMJ Bioengineering Conference, 2014.

Kerwell, S., Alfaro, M., Pourzal, R., Mercuri, L. G., Sukotjo, C., Mathew, M. T.: Examination of Retrieved Temporomandibular Joint Implants: Failure Mechanisms, Condylar Resorption: Orthodontic and Surgical Management Perspectives, 2014.

Kerwell, S., Baer, D., Martin, E., Shull, K., Mathew, M. T.: Electrochemically Induced Film Formation on CoCrMo Alloy for Hip Joint Applications, Rush University Research Symposium, 2014.

PUBLICATIONS: M. Mathew, S. Kerwell, H. Lundberg, C. Sukotjo, L. G. Mercuri, "Tribocorrosion and oral and maxillofacial surgical devices," British Journal of Oral and Maxillofacial Surgery, vol. 52, issue 5, May 2014.